J. Fluid Mech. (1989), *vol.* 201 *pp.* 447–483
Printed in Great Britain

On the three families of instability waves of high-speed jets

By CHRISTOPHER K. W. TAM AND FANG Q. HU
Department of Mathematics, Florida State University, Tallahassee, FL 32306-3027, USA

(Received 11 April 1988 and in revised form 6 October 1988)

In this paper the normal-mode small-amplitude waves of high-speed jets are investigated analytically and computationally. Three families of instability waves, each having a distinct wave pattern and propagation characteristics, have been found. One of the families of waves is the familiar Kelvin–Helmholtz instability wave. The other two families of waves do not appear to have been clearly identified and systematically studied before. Waves of one of the new wave family propagate with supersonic phase velocities relative to the ambient gas. They are, therefore, referred to as supersonic instability waves. Waves of the other family have subsonic phase velocities. Accordingly they are called subsonic waves. The subsonic waves have the unusual property that they are unstable only for jets with finite thickness mixing layers. They are neutral waves when calculated by a vortex-sheet jet model.

Earlier Oertel (1979, 1980, 1982) using a novel optical technique observed in a series of experiments three sets of waves in high-speed jets. The origin of these waves, however, remains so far unexplained and a theory has yet to be developed. In the present study it will be shown that the computed wave patterns and propagation characteristics of the Kelvin–Helmholtz, the supersonic and the subsonic instability waves match essentially those observed by Oertel. The physical mechanisms which give rise to the three families of waves as well as some of the most salient characteristic features of each set of waves are discussed and reported here.

1. Introduction

Recently Oertel (1979, 1980, 1982) carried out a series of experimental studies on the instability waves of high-speed jets. In his experiments the jets were formed by hot or cold gases issued through convergent–divergent nozzles mounted at the end of a shock tube. Observations indicated that these shock-tube generated jets had very uniform cores surrounded by thin mixing layers. By using a novel optical technique, Oertel was able to identify three families of waves in his jets. Each family of waves had its distinct characteristics and propagation speed. Pictures of these waves are shown in figure 1. Associated with the first set of waves (labelled W') is a strong acoustic near field. In the region immediately outside the jet the waves appear as nearly parallel straight lines trailing the flow of the jet. This near-field wave pattern was observed by several investigators earlier while studying the topic of sound generation by instability waves (e.g. Lowson & Ollerhead 1968; Rosales 1970; Tam 1971; Chan & Westley 1973). Tam (1971) and later Chan & Westley (1973) suggested and showed that this near-field acoustic wave pattern was generated by the Kelvin–Helmholtz instability waves of the flow. By using a vortex-sheet model they were able to calculate correctly the angle of inclination and the speed of

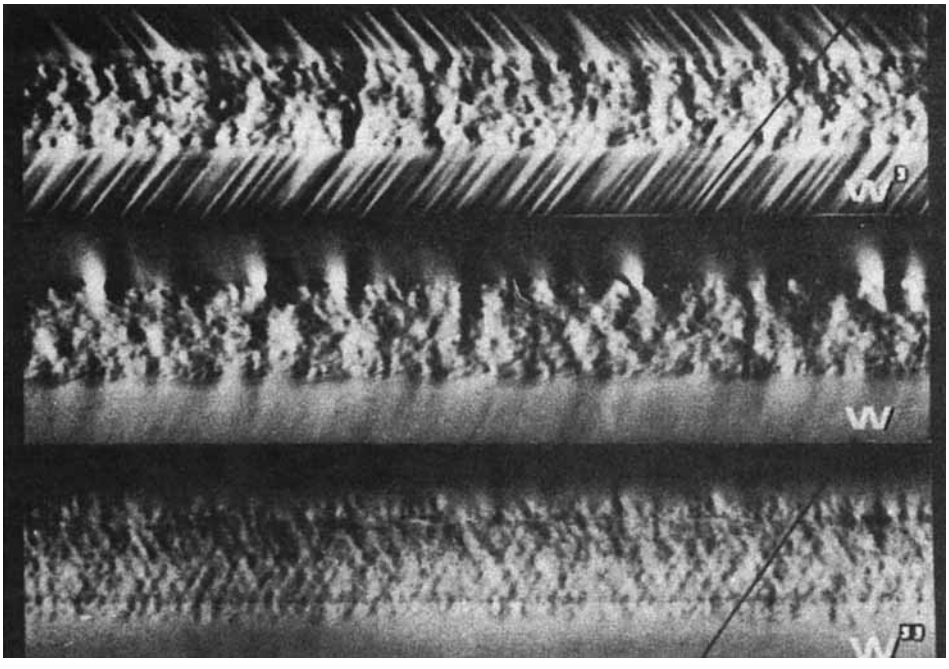

FIGURE 1. Pictures showing the wave patterns of the three sets of waves observed by Oertel (1980) in high-speed jets. Flow is from left to right. (Reproduced with permission.)

propagation of the wavefronts. Thus the first family of instability waves observed by Oertel is the familiar Kelvin–Helmholtz instability.

The second family of waves observed by Oertel (labelled W in figure 1) has a near acoustic field in which the wavefronts are almost normal to the jet boundary. Within the range of jet flow parameters covered in Oertel's experiment the propagation speed of this set of waves is found to be less than that of the Kelvin–Helmholtz instability waves. The third family of waves (labelled W'' in figure 1), unlike the first two sets of waves, appears to have no near field. The waves seem to be confined primarily inside the jet. Within the jet the waves display a characteristic cross-hatched pattern. To the best of our knowledge, no one has made a clear identification or association of these last two families of waves to any known instability of high-speed jets. One of the main objectives of this paper is to provide a theoretical foundation to these waves. It will be shown theoretically that a high-speed jet with thin mixing layers can support three distinct families of instability waves. These waves exhibit near-field patterns and propagation characteristics which match those observed by Oertel (1979, 1980, 1982) and others (in those cases of Kelvin–Helmholtz instability).

Before embarking on an analysis of the instability wave modes of high-speed jets it is found useful first to examine physically why these jets can support three distinct families of waves. Earlier Ackeret (see Liepmann & Puckett 1947; Papamoschou & Roshko 1986) had provided a physical explanation of the mechanism responsible for the Kelvin–Helmholtz instability in a thin shear layer. Here it will be shown that Ackeret's physical argument can be extended to the case of high-speed jets to explain why these jets can sustain three classes of waves. For the sake of

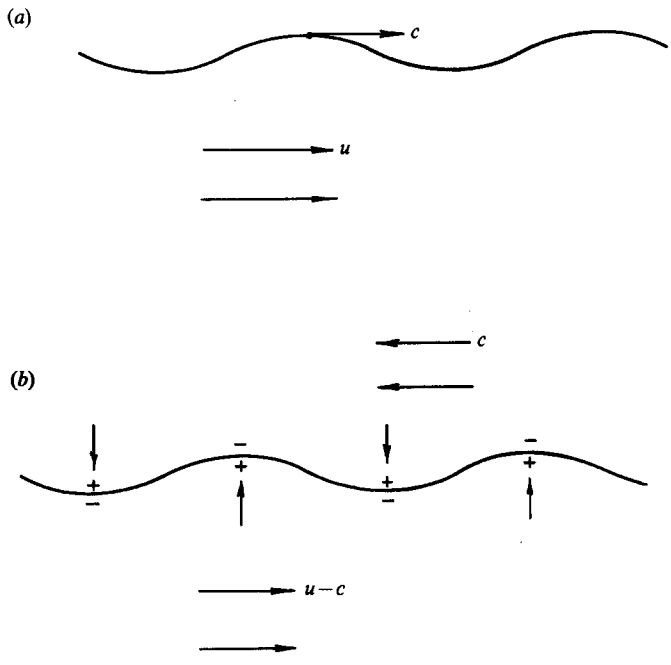

FIGURE 2. Kelvin–Helmholtz instability mechanism at subsonic Mach number. +, high pressure region; −, low pressure region. (*a*) Stationary frame of reference. (*b*) Wave frame of reference.

completeness Ackeret's explanation of the Kelvin–Helmholtz instability mechanism will be briefly reviewed.

Consider a two-dimensional vortex sheet separating a fluid at rest and a fluid moving at a subsonic velocity U. It will be assumed that the vortex sheet is deformed by a Kelvin–Helmholtz wave with a phase velocity c as shown in figure 2 (*a*). Ackeret suggested that one should view the flow not in the stationary frame of reference but in a moving frame travelling with the phase velocity c of the wave. In this wave frame the flow is as shown in figure 2 (*b*). Now for the flow above the vortex sheet, the vortex sheet may be regarded as a wavy wall. So within a quasi-steady approximation the flow is that of a uniform flow past a wavy wall. The solution of this problem is well known (see e.g. Liepmann & Roshko 1957, ch. 8). At subsonic Mach number the pressure is lowest at the crests of the wavy wall and highest at the troughs. Similar consideration may also be applied to the flow below the vortex sheet. Again the pressure is lowest at the crests and highest at the troughs. Since the crests and troughs interchange on the two sides of the vortex sheet the result is that a net pressure imbalance would exist across the thin mixing layer in the quasi-steady approximation. This pressure imbalance is in phase with the vortex-sheet displacement and hence would tend to increase its amplitude leading to the well-known Kelvin–Helmholtz instability

Now suppose the Mach number of the flow is highly supersonic so that in the wave frame of reference the flows on the two sides of the vortex sheet are supersonic as shown in figure 3. For supersonic flow over a wavy wall it is known that the pressure distribution is no longer in phase but rather 90° out of phase with the displacement of the wall. This results in identical pressure distribution on both sides of the vortex

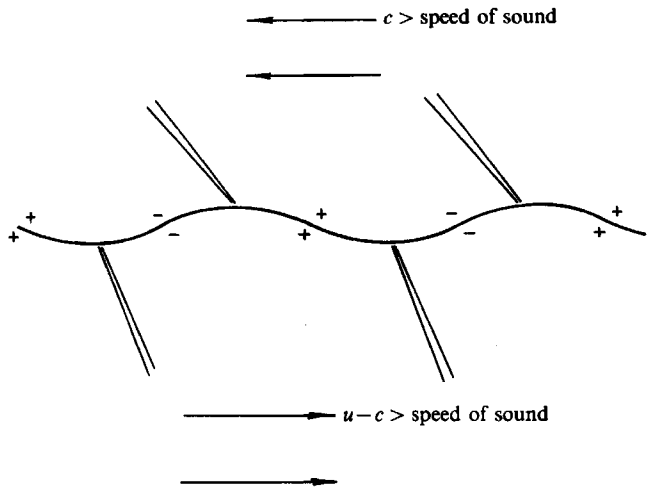

FIGURE 3. Pressure distribution on the two sides of a vortex-sheet layer at supersonic convective Mach numbers as viewed in the wave frame of reference. +, high-pressure region; −, low-pressure region.

sheet. The net effect is that the wave becomes neutrally stable. This is in agreement with the prediction of Miles (1958) using hydrodynamic stability theory.

For circular jets the situation is somewhat different. The cylindrical vortex sheet which bounds the jet also tends to reflect acoustic disturbances which impinge on it. Thus acoustic disturbances could be trapped inside the jet bouncing back and forth forming a periodic Mach wave system as shown in figure 4. The condition under which such a Mach wave system can exist is that in the wave frame of reference the flow inside the jet is supersonic. Since acoustic disturbances can propagate upstream (the phase velocity c of the wave is negative in this case) or downstream (c is positive) relative to the flow of the jet, this type of Mach wave system exists in supersonic as well as subsonic jets as long as $u_j - c$ is greater than the speed of sound where u_j is the jet velocity. Of course, for subsonic jets c would have to be negative, namely, the wave is an upstream propagating wave. The pressure distribution associated with a Mach wave system inside a cylindrical wavy wall is given in the Appendix. It is easy to see from the formula given there, equation (A 3), that depending on the wavelength, the pressure distribution may be 180° out of phase with the radial vortex-sheet displacement. The wave speed c may, however, be subsonic or supersonic relative to the ambient gas. Let us first consider the case of subsonic waves. In the wave frame of reference the ambient flow is subsonic. The pressure distribution associated with subsonic flow outside a wavy cylinder may be found in the Appendix, equation (A 4). Not surprisingly, the pressure is 180° out of phase with the radial displacement of the cylindrical wavy wall. Thus, by suitable choice of the wavelength of the Mach wave system, pressure balance on the two sides of the thin mixing layer of the jet is possible (see figure 4*a*). This implies that the vortex-sheet jet can support a family of neutral waves. For supersonic jets it will be shown later in this paper that if the effect of finite mixing-layer thickness is included this family of waves actually are unstable. Clearly with subsonic phase velocity relative to the ambient gas the amplitudes of these waves must decay exponentially in the radial direction outside the jet. In other words the disturbances associated with this family of waves are confined mainly inside the jet. These subsonic waves are the third

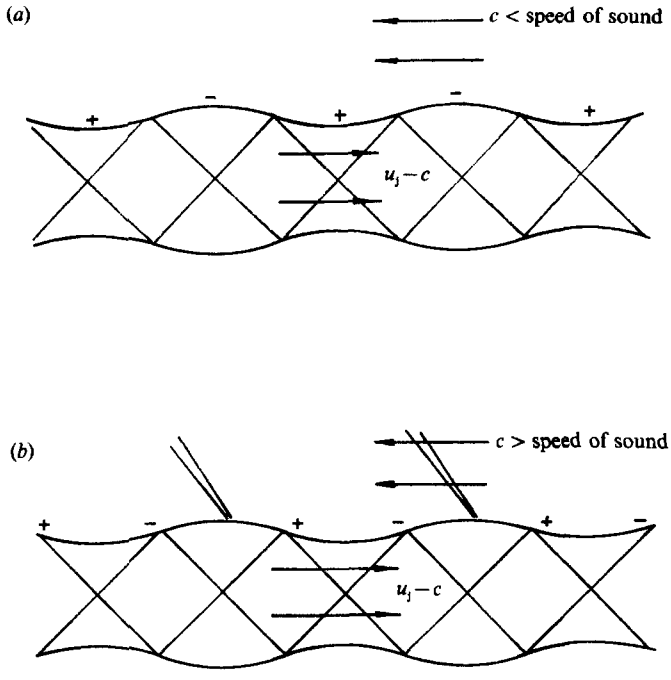

FIGURE 4. Pressure distribution on the outside surface of a cylindrical wavy vortex sheet jet as viewed in the wave frame of reference. Also shown is a Mach wave system inside the jet. (*a*) Subsonic flow outside. (*b*) Supersonic flow outide.

family of waves observed by Oertel (1980). To distinguish the waves of this family from the other two they will be referred to as the subsonic (instability) waves in the rest of this paper.

For very high-speed jets the phase velocity, c, of the Mach wave system may become supersonic relative to the ambient gas. In this case the flow is supersonic both inside and outside the jet with respect to the wave frame as shown in figure 4(*b*). The pressure distribution associated with a steady supersonic flow over a cylindrical wavy wall has been determined in the Appendix, equation (A 6). On comparing the pressure distribution formulae inside and outside the cylindrical vortex sheet it is evident that pressure balance is impossible regardless of the choice of wavelength. Hence unlike the case of subsonic waves no neutral waves are possible. Further it is easy to show that for certain wavelengths a pressure imbalance which is in phase with the vortex-sheet displacement is possible. The net result is that with the internal Mach wave system a highly supersonic jet can sustain a family of instability waves with supersonic phase velocities. With supersonic phase velocity relative to the ambient gas the instability wave will generate a Mach-wave-like near field as discussed by Tam (1971) and Chan & Westley (1973). In a later section of this paper is will be shown that the calculated phase velocities of these waves are in agreement with the measured phase velocities of Oertel's second family of waves. Because of their supersonic phase velocities these waves will be called the supersonic instability waves.

In a study of the instabilities of top-hat profile jets Gill (1965) appeared to be the first to notice that there were instability wave modes other than the well-known Kelvin–Helmholtz instability wave. Gill reasoned that these additional waves were

resonances and referred to them as reflection modes. He suggested that these resonances arose when sound waves impinged on the vortex sheet at certain critical angles. The impingement caused the release of a large amount of energy from the thin shear layer. Presumably, although it was never elaborated by him, the released energy increased the amplitude of the acoustic waves and hence led to instabilities. Recently, motivated by possible application to jet-like galactic structures, Ferrari, Trussoni & Zaninetti (1981), Cohn (1983), Payne & Cohn (1984) and Zaninctti (1986, 1987), following the suggestion of Gill, investigated the 'reflection modes' of very high-speed jets. Their studies were unfortunately somewhat restricted and except for Payne & Cohn focused primarily on temporal instabilities. It is to be noted that in Oertel's experiments the observed instabilities were spatial instability waves. In addition, their calculated results also appeared to be quite fragmentary, and confined essentially to vortex-sheet jets. No distinctions between subsonic and supersonic instability waves were made so that it would not be possible through these works to deduce that high-speed jets can support three distinct families of instabilities. Recently it was found that the Mach wave mechanism which gave rise to supersonic instability waves in a jet also produced similar instabilities in the case of a plane shear layer enclosed inside a rectangular channel. Extra complications, however, arise from coupling to the intrinsic neutral acoustic modes of the channel. This problem has now been studied and clarified by the present authors (Tam & Hu 1988).

In this paper it will be shown that high-speed jets are subjected to three families of instabilities. One of these is the familiar Kelvin–Helmholtz instability waves. The other two are generated by the presence of a Mach wave system inide the jet. In jets with infinitesimally thin mixing layers the subsonic waves are neutrally stable. These waves are unstable only if a finite-thickness shear layer is included in the mathematical model. The wave patterns associated with the spatial instabilities of the three families of waves will be analysed and compared with experimental observations. It will also be shown that at sufficiently high Mach number the growth rate of the Kelvin–Helmholtz instability decreases drastically. At still higher Mach number this wave mode would merge with the supersonic instability waves. When this happens the Kelvin–Helmholtz mode can no longer be readily identified. Other important characteristics of the three families of instability waves will be reported in §§3–7 of this paper.

2. The three families of instability waves of high-speed jets

In the past numerous studies of the Kelvin–Helmholtz instability waves of compressible jets have been carried out. References to some of the more recent works can be found in Michalke (1984), Tam & Burton (1984), Zaninetti (1986, 1987) and others. Most of these investigations, however, focused primarily on the Kelvin–Helmholtz instability in subsonic and low supersonic jets. Here our principal interest is on the other two families of instability waves of high-speed jets observed by Oertel (1979, 1980, 1982). In this work a vortex-sheet jet model as well as a more realistic jet model with continuous velocity profile and finite shear-layer thickness will be used. Experience indicates that the simpler vortex-sheet model can usually provide reasonably good estimates of the phase velocity of an instability wave. But for the purpose of calculating accurately the growth rate of the wave, a finite-thickness jet model is necessary. In later sections of this paper it will be shown that if the vortex-sheet model of a supersonic jet is used the growth rates of subsonic waves are found to be zero, i.e. they are neutral waves. On the other hand,

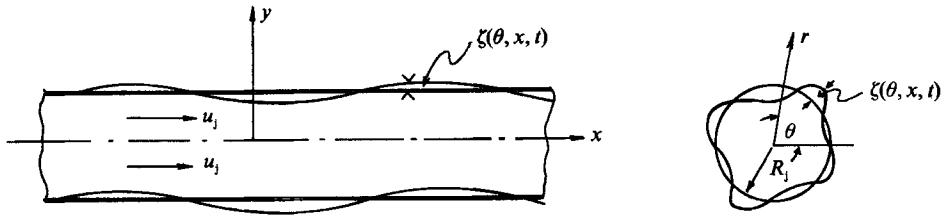

FIGURE 5. Perturbed motion of a round jet bounded by a vortex sheet.

calculations based on the more realistic finite mixing-layer thickness model reveal that these are unstable waves with finite spatial growth rates. For this reason, all the three families of waves will be referred to as unstable waves even in the context of the vortex-sheet jet model.

2.1. *Vortex-sheet model of high-speed jets*

Consider a supersonic jet of velocity u_j and radius R_j bounded by a vortex sheet as shown in figure 5. Let (r, θ, x) be a cylindrical coordinate system centred at the axis of the jet with the x-axis pointing in the direction of the flow. On starting from the linearized continuity, momentum and energy equations of a compressible inviscid fluid, it is straightforward to find that the pressure associated with small-amplitude disturbances superimposed on the mean flow inside and outside the jet, p_i and p_o, are governed by the wave and convective wave equation respectively.

$$\frac{\partial^2 p_o}{\partial t^2} - a_o^2 \nabla^2 p_o = 0 \quad (r \geqslant R_j), \tag{2.1}$$

$$\left(\frac{\partial}{\partial t} + u_j \frac{\partial}{\partial x}\right)^2 p_i - a_j^2 \nabla^2 p_i = 0 \quad (r \leqslant R_j), \tag{2.2}$$

where a_o and a_j (subscripts o and j denote physical quantities outside and inside the jet) are the speeds of sound outside and inside the jet. Let $\zeta(\theta, x, t)$ be the radial displacement of the vortex sheet. The dynamic and kinematic boundary conditions at the vortex sheet $r = R_j$ are

$$p_i = p_o, \quad -\frac{1}{\rho_o}\frac{\partial p_o}{\partial r} = \frac{\partial^2 \zeta}{\partial t^2}, \quad -\frac{1}{\rho_j}\frac{\partial p_i}{\partial r} = \left(\frac{\partial}{\partial t} + u_j \frac{\partial}{\partial x}\right)^2 \zeta. \tag{2.3, 2.4, 2.5}$$

It is straightforward to find that separable solutions of the above equations and boundary conditions which also satisfy the boundedness condition at $r = 0$ and $r \to \infty$ are

$$\begin{pmatrix} p_o \\ p_i \end{pmatrix} = \begin{pmatrix} H_n^{(1)}(\mathrm{i}\eta_o r) \\ H_n^{(1)}(\mathrm{i}\eta_o R_j)\, J_n(\eta_i r)/J_n(\eta_i R_j) \end{pmatrix} \mathrm{e}^{\mathrm{i}(kx + n\theta - \omega t)}, \tag{2.6}$$

where $\eta_o = (k^2 - \omega^2/a_o^2)^{\frac{1}{2}}$, $\eta_i = ((\omega - u_j k)^2/a_j^2 - k^2)^{\frac{1}{2}}$. The branch cuts of η_o and η_i are taken to be

$$-\tfrac{1}{2}\pi < \arg \eta_o \leqslant \tfrac{1}{2}\pi, \quad 0 \leqslant \arg \eta_i < \pi.$$

The wavenumber and angular frequency k and ω are related by the eigenvalue relation

$$D(\omega, k) \equiv \frac{\mathrm{i}\eta_o}{\rho_o \omega^2} J_n(\eta_i R_j) H_n^{(1)\prime}(\mathrm{i}\eta_o R_j) - \frac{\eta_i}{\rho_j (\omega - u_j k)^2} H_n^{(1)}(\mathrm{i}\eta_o R_j) J_n'(\eta_i R_j) = 0, \tag{2.7}$$

($'$ = derivative).

Equation (2.7) is not new (see e.g. Tam 1971; Chan & Westley 1973). Solutions of (2.7) or the roots of $D(w, k)$ are the wave modes of the jet. The nature of these wave modes will be discussed in subsequent sections of this paper.

2.2. *Finite-thickness shear-layer model*

In a real jet the mean velocity and density profiles are continuous. Experimentally it has been found that the flow velocity is uniform in the central part of the jet. Surrounding this uniform core is a mixing layer with a velocity profile which can be closely approximated by a half-Gaussian function, see e.g. Troutt & McLaughlin (1982). Thus the mean velocity profile in the core region of the jet will be taken as

$$\bar{u} = \begin{cases} u_j & (r < h), \\ u_j \exp\left[-(\ln 2)\left(\dfrac{r-h}{b}\right)^2\right] & (r \geqslant h), \end{cases} \tag{2.8}$$

in the present calculation. In (2.8) h is the radius of the uniform core and b is the half-width of the jet mixing layer. The parameters h and b are related by the condition of conservation of momentum flux

$$\int_0^\infty \bar{\rho}\bar{u}^2 r \,\mathrm{d}r = \tfrac{1}{2}\rho_j u_j^2 R_j^2. \tag{2.9}$$

The mean density $\bar{\rho}$ is related to the mean velocity $\bar{u}$ by the Crocco's relation (Prandtl number is assumed to be unity).

It is easy to show starting from the linearized equations of motion for an inviscid, non-conducting compressible fluid that the equation governing the perturbation pressure p is (see e.g. Tam & Burton 1984)

$$p(r, \theta, x, t) = \hat{p}(r) \exp\left[\mathrm{i}(kx + n\theta - \omega t)\right], \tag{2.10}$$

$$\frac{\mathrm{d}^2\hat{p}}{\mathrm{d}r^2} + \left[\frac{1}{r} - \frac{1}{\bar{\rho}}\frac{\mathrm{d}\bar{\rho}}{\mathrm{d}r} + \frac{2k}{\omega - \bar{u}k}\frac{\mathrm{d}\bar{u}}{\mathrm{d}r}\right]\frac{\mathrm{d}\hat{p}}{\mathrm{d}r} + \left[\frac{(\omega - \bar{u}k)^2}{\bar{a}^2} - \frac{n^2}{r^2} - k^2\right]\hat{p} = 0, \tag{2.11}$$

where $\bar{a} = (\gamma p_0/\bar{\rho})^{\frac{1}{2}}$. The locally parallel flow approximation has been invoked in deriving (2.11). This equation together with the boundedness condition at $r = 0$ and $r \to \infty$ form an eigenvalue problem for $\omega = \omega(k)$ or $k = k(\omega)$. The eigenvalue can be determined by integrating this equation numerically. Details of the numerical procedure may be found in Tam & Burton (1984) and will not be elaborated here. To initiate the iteration cycle of the numerical procedure the solution of the vortex-sheet jet model has been used throughout this paper.

2.3. *Existence of three families of wave solutions*

The branch points of the function $\mathrm{i}\eta_0$ and η_i of (2.7) for a given real value of k in the complex ω-plane are,

$$\omega = \pm ka_0, \quad \omega = ka_j(u_j/a_j \pm 1), \tag{2.12}$$

respectively. The branch cuts of these functions are shown in figure 6. The significance of the branch points is that regions of the complex ω-plane to the left-hand branch point represents waves for which the flow has supersonic convective Mach number. Convective Mach number is defined as the Mach number of the flow measured in the moving frame of the wave. It is straightforward to show that for every point in this region of figure 6(*b*) the supersonic convective Mach number relationship $u_j - \omega_r/k > a_j$ holds ($\omega = \omega_r + \mathrm{i}\omega_i$), where subscripts r and i denote real

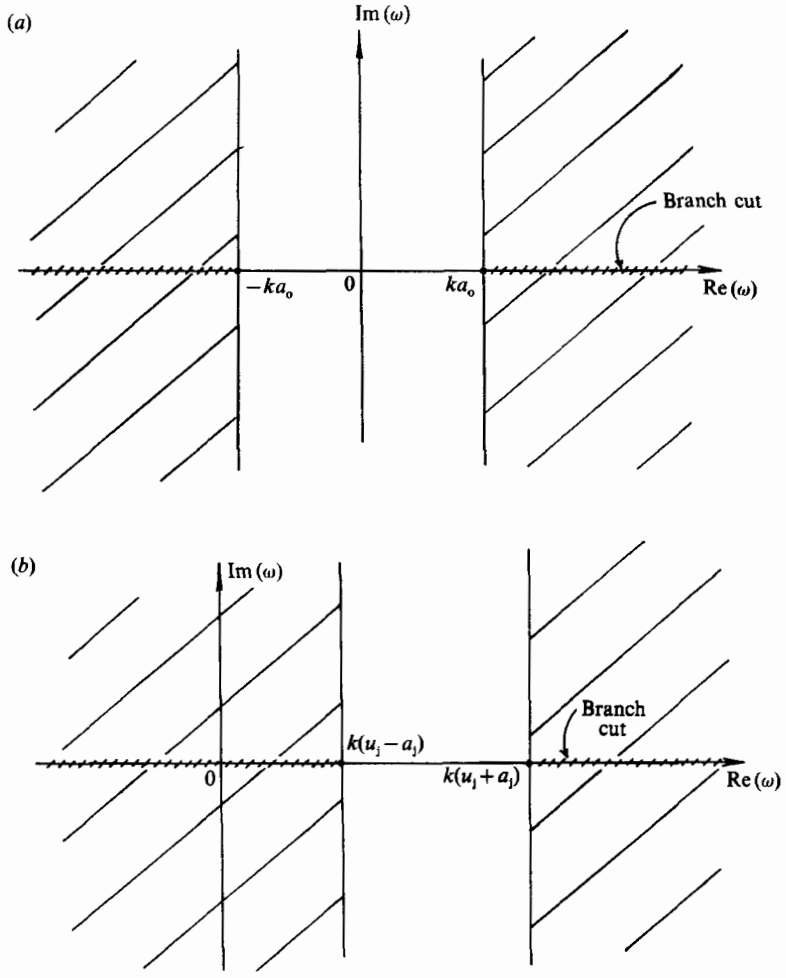

FIGURE 6. Branch cuts of (*a*) $i\eta_o$ and (*b*) η_i in the complex ω-plane for a supersonic jet. Shaded areas are regions with supersonic convective Mach number.

and imaginary parts. Similarly for every point to the left of the left-hand branch point of $i\eta_o$ in figure 6(*a*) which is for the static environment outside the jet the inequality $|\omega_r/k| > a_o$ applies.

It is also easy to show that points in the region of the complex ω-plane to the right of the right-hand branch points in figure 6 again represent waves for which the convective Mach number of the flow is supersonic. In this case the inequalities are,

$$\omega_r/k - u_j > a_j, \quad \omega_r/k > a_o,$$

inside and outside the jet respectively. The remaining region of the complex ω-plane, namely, the vertical strip between the two branch points represents waves having subsonic convective Mach numbers.

According to the instability mechanism described in the previous section, supersonic instability waves exist in a jet only if the convective Mach numbers (for the flow inside and outside the jet) are supersonic. In terms of the complex ω-plane this is possible only if the jet Mach number is highly supersonic such that the left-

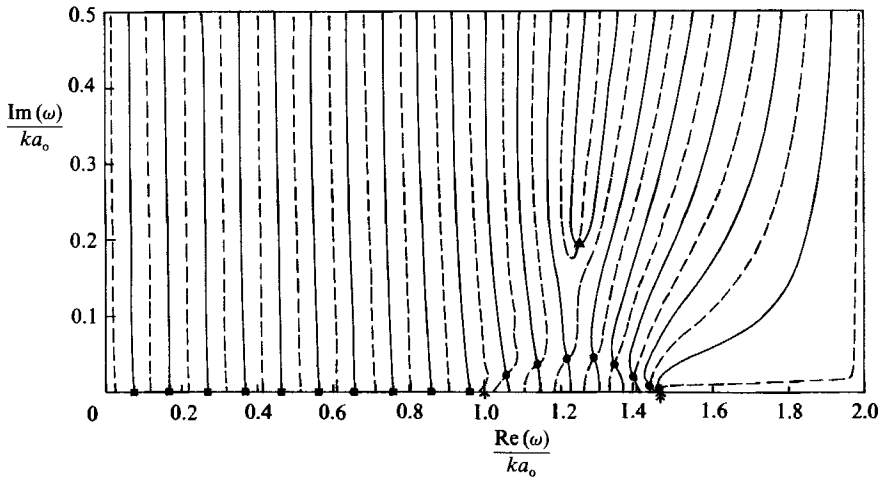

FIGURE 7. Zeros of the dispersion function $D(\omega, k)$ in the complex ω-plane. $M_j = 4.0$, cold jet, $kR_j = 15.0$, $n = 0$ mode. ——, $\mathrm{Re}\,(D) = 0$; – – –, $\mathrm{Im}\,(D) = 0$. ↑, right-hand branch point of $i\eta_0$, ↕, left-hand branch point of η_i. ▲, Kelvin–Helmholtz instability; ●, supersonic instabilities; ■, subsonic wave modes.

hand branch point of figure 6(*b*) lies to the right of the right-hand branch point of figure 6(*a*), In other words,

$$u_j > a_j + a_0. \tag{2.13}$$

The vertical strip between the two branch points satisfies the supersonic convective Mach numbers criterion.

Now for a vortex-sheet supersonic jet the instability wave modes are given by the zeros of the dispersion function, $D(\omega, k)$, of (2.7). To locate the zeros in the complex ω-plane for a given value of k, the following grid-search method has been found useful. To implement this method the region of interest in the ω-plane is first subdivided into small subregions by a rectangular grid. The value of the dispersion function $D(\omega, k)$ of equation (2.7) are calculated at each grid point. A plotting subroutine is then called which performs a two-dimensional interpolation of this set of values and constructs the two families of curves $\mathrm{Re}\,(D) = 0$ and $\mathrm{Im}\,(D) = 0$. The intersection of these curves provide a first estimate of the locations of the zeros of D. These values are then refined by applying Newton's iteration method.

Figure 7 shows a typical example of the zeros of the dispersion function $D(\omega, k)$ found by the grid-search method for a highly supersonic jet. In this example the axisymmetric waves ($n = 0$) of a Mach number 4.0 cold jet are considered. The wavenumber kR_j, has been set to be equal to 15.0 in the calculation. It is evident in this figure that there are three families of zeros, or wave modes. The isolated zero with the largest temporal growth rate is the familiar Kelvin–Helmholtz instability. Immediately below the Kelvin–Helmholtz zero is a family of zeros lying in the vertical strip (with $\mathrm{Im}\,(\omega) > 0$) between the right-hand branch point of $i\eta_0$ and the left-hand branch point of η_i. These are the supersonic instability waves. To the left of the supersonic instability waves is another family of zeros. These zeros lie on the real ω-axis between the two branch points $\omega/k = \pm a_0$. These waves, therefore, have subsonic phase velocity relative to the ambient speed of sound. They are the subsonic waves. For non-axisymmetric wave modes with $n = 1, 2, 3, \ldots$, maps similar to figure 7 have been constructed by the grid-search method. Again they exhibit three sets of

wave modes resembling those in figure 7. The above results apply to hot jets as well. For hot jets the supersonic instability wave modes exist even at much lower supersonic Mach number. When condition (2.13) is not satisfied, only the Kelvin–Helmholtz and the subsonic waves could be found. Experimentally Oertel (1979, 1980, 1982) found that his second set of waves (the W waves) exist only when $u_j > a_j + a_o$, independent of Mach number and the type of gas used to form the jet. This is in total agreement with condition (2.13). Further comparisons between computed wave characteristics and experimental measurements of the three families of waves of high-speed jets will be reported later.

2.4. *Relationship between Kelvin–Helmholtz instability and supersonic instability waves at high-jet Mach number*

It has been known since the early work of Miles (1958) that the growth rate of the Kelvin–Helmholtz instability decreases as the flow Mach number increases. Thus at higher jet Mach number one would expect the Kelvin–Helmholtz zero in figure 7 to move towards the real ω-axis. However, between the real ω-axis and the Kelvin–Helmholtz zero are the supersonic instability wave modes. An interesting question, therefore, arises as to whether the Kelvin–Helmholtz zero would pass through the supersonic instability wave modes to reach the ω-axis. To answer this question a series of maps similar to figure 7 has been calculated with a fixed wavenumber but increasing jet Mach number. Attention is focused on the trajectory of the Kelvin–Helmholtz zero in the complex ω-plane as the jet Mach number increases. It is found that when the Mach number reaches a certain critical value the Kelvin–Helmholtz zero blends itself into the supersonic instability wave modes. At still higher jet Mach number the Kelvin–Helmholtz mode seems to lose its identity and cannot be readily singled out. The wave mode merging phenomenon is illustrated in figure 8. In this example the calculations are for the axisymmetric mode ($n = 0$) and $kR_j = 15.0$. Figure 8(a) shows the curves $\mathrm{Re}\,(D) = 0$ and $\mathrm{Im}\,(D) = 0$ in the complex ω-plane at jet Mach number 4.4. The zero of $D(\omega, k)$ with the largest imaginary part is the Kelvin–Helmholtz mode. Figure 8(b) shows a similar map at jet Mach number 4.6. Now as Mach number increases from 4.4 to 4.6 drastic changes of the curves $\mathrm{Re}\,(D) = 0$ and $\mathrm{Im}\,(D) = 0$ take place around 4.5. As a result it is no longer possible to single out readily which is the Kelvin–Helmholtz mode in figure 8(b). Figure 8(c) gives the locations of the supersonic instability wave modes at Mach number 5.0. No trace of a distinct Kelvin–Helmholtz mode can be found. In other words, the merging of the Kelvin–Helmholtz mode with the supersonic instability wave modes is complete. An examination of the eigenfunctions of the wave modes seems to reinforce this conclusion. At Mach number above a critical value all the eigenfunctions exhibit similar characteristics whereas at lower Mach numbers the eigenfunction of the Kelvin–Helmholtz wave is distinctly different from those of the supersonic instability waves. Typical eigenfunction distribution will be provided later.

Extensive numerical computations indicate that the critical Mach number, M_c, above which the Kelvin–Helmholtz mode blends itself completely with the supersonic instability wave modes is insensitive to the azimuthal wavenumber n and the axial wavenumber k. (Note: M_c does not have a sharply defined value but can be narrowed down to a very narrow range.) It turns out that M_c is affected mainly by the jet temperature. Figure 9 shows the dependence of M_c on the jet to ambient temperature ratio. In constructing this graph the ratios of the specific heats of the gases inside and outside the jet have been assumed to be the same. As can be seen M_c decreases with

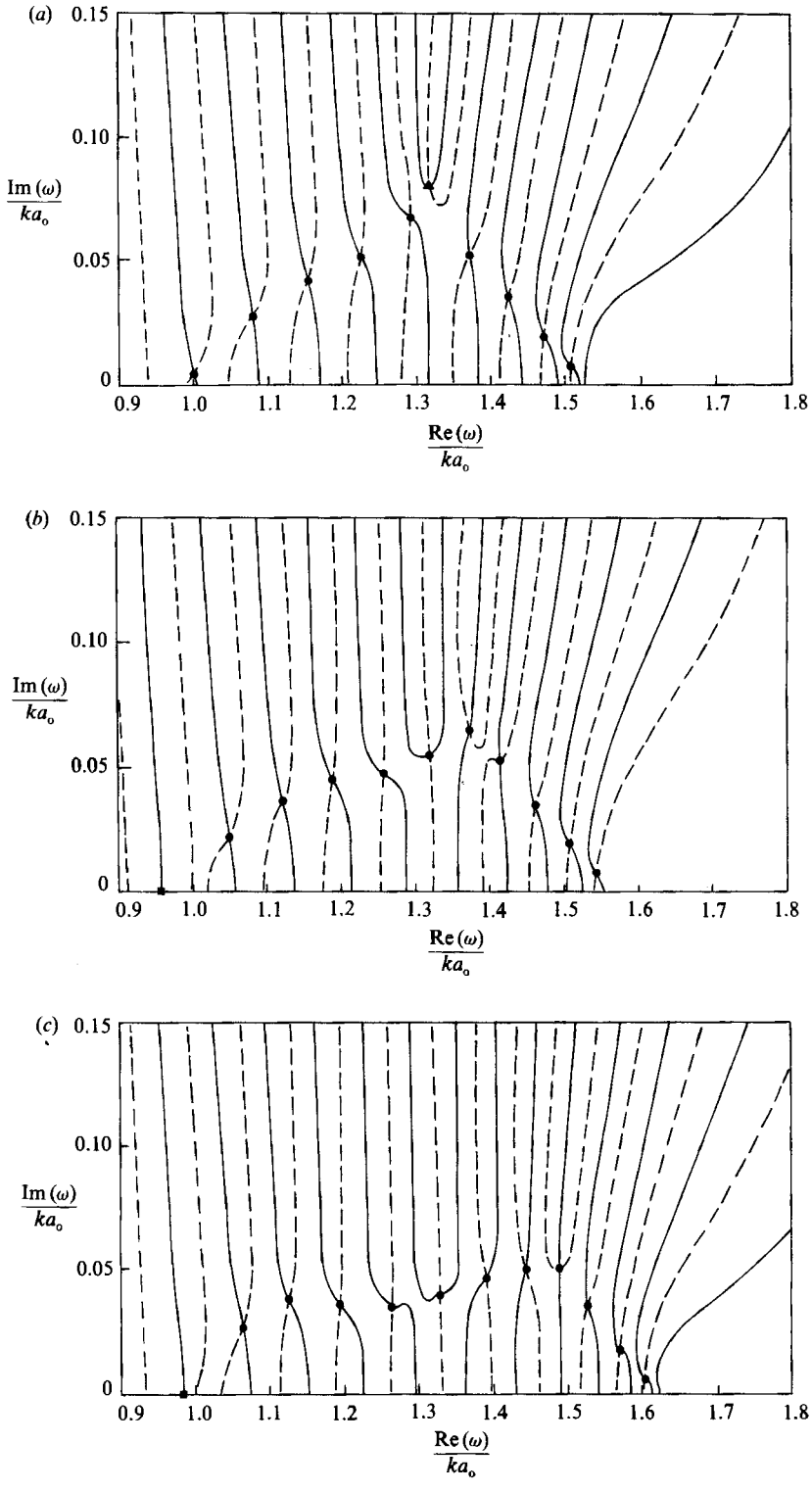

FIGURE 8. Location of the zeros of D in the complex ω-plane. Cold jet, $kR_j = 15.0$. ——, $\mathrm{Re}\,(D) = 0$; – – –, $\mathrm{Im}\,(D) = 0$. ●, supersonic instability wave; ▲, Kelvin–Helmholtz instability wave; ■, subsonic wave. (*a*) $M_j = 4.4$. (*b*) $M_j = 4.6$. (*c*) $M_j = 5.0$.

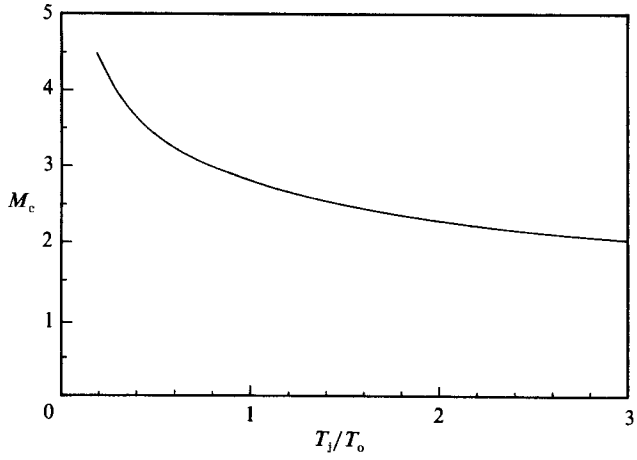

FIGURE 9. Critical Mach number above which the Kelvin–Helmholtz instability wave can no longer be identified as a function of jet to ambient temperature ratio (T_j/T_o).

an increase in jet temperature. It appears that the curve tends to an asymptote as the temperature ratio becomes very large.

3. Spatial instability

In this work the primary interest is the spatial instability wave modes. These, rather than the temporal instabilities, are the waves observed in Oertel's (1979, 1980, 1982) experiments. For spatial instability waves ω is real. However, it is known that in determining these waves it is not sufficient to set ω to a real number and look for the zeros or poles of $D(\omega, k)$ in the complex k-plane. One must recognize that waves can propagate in the positive or negative x-direction. Such a distinction is absolutely necessary. Failure to do so may erroneously treat an evanescent wave as a spatially amplifying wave and vice versa. Here the criterion for distinguishing between an evanescent and a spatially amplifying wave established by Briggs (1964) will be followed. According to Briggs, if one is interested in spatial instability waves of frequency Ω one should start calculating the roots of the dispersion function by setting the real part of ω equal to Ω and the imaginary part of ω to be a large positive value. Zeros of $D(\omega, k)$ lying in the upper half k-plane represent waves propagating in the positive x-direction while those in the lower half k-plane represent waves propagating in the negative x-direction. Figure 10 shows a typical example. Here the calculation is for a cold jet of Mach number 4.0 with $\omega R_j/u_j = 2.6 + 1.5\mathrm{i}$. The zeros of $D(\omega, k)$ in the k-plane are located by the grid-search procedure described above. In figure 10 these zeros are denoted by open circles. Also shown in this figure are the branch cuts of η_o and η_i denoted by double thin lines. The branch points of η_o and η_i in the complex k-plane are $\pm\omega/a_o$ and $\omega/(u_j \pm a_j)$ respectively. Now to obtain the normal mode solutions the point ω must be pushed towards the real axis. Here real ω is kept fixed in the complex ω-plane throughout the entire contour deformation process. Numerically this is carried out by reducing the imaginary part of ω by small increments until it is equal to zero (solid circles). For each intermediate value of ω the grid-search procedure is implemented. In this way the movement of all the zeros of $D(\omega, k)$ can be traced as $\mathrm{Im}\,(\omega) \to 0^+$. The trajectories of the zeros are shown in figure 10. The final locations of the zeros, i.e. when ω is real, are denoted by solid circles and

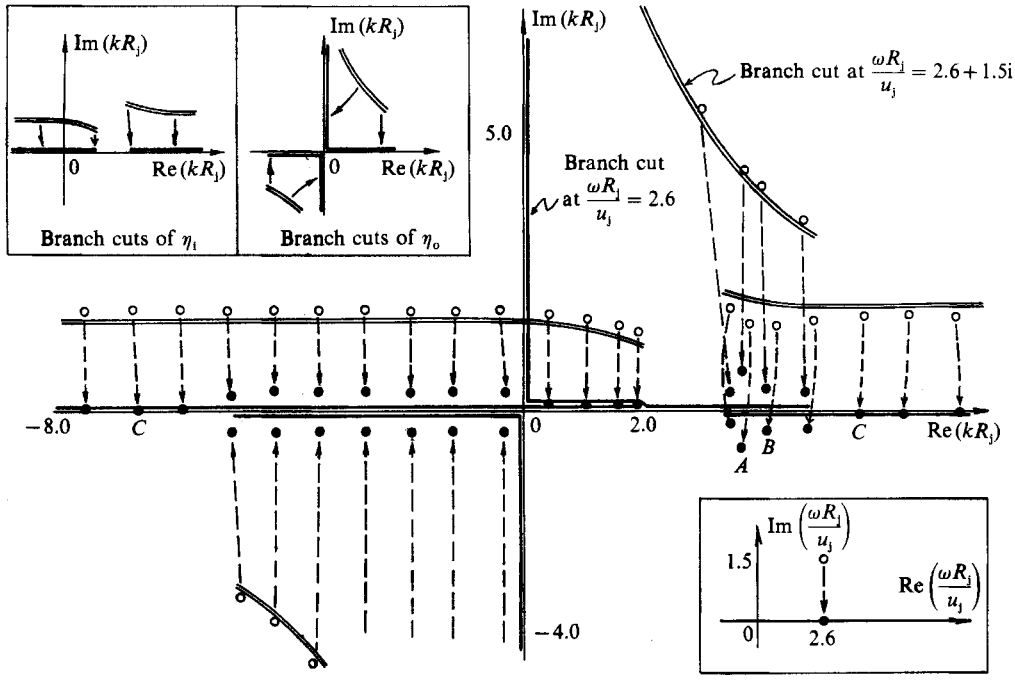

FIGURE 10. Trajectories of the zeros of $D(\omega, k)$ in the complex k-plane as $\mathrm{Im}(\omega) \to 0^+$ showing the Kelvin–Helmholtz instability wave (A)., the supersonic instability waves (B), and the subsonic waves (C). Cold jet, Mach number 4.0, $n = 0$.

the branch cuts by solid black lines. Some of the zeros in the vertical strip between the right-hand branch points of η_i and η_o crossed into the lower half k-plane as ω is pushed toward the real axis. These are the spatial supersonic instability wave modes. The isolated zero of $D(\omega, k)$ with the largest negative imaginary part which crosses into the lower half k-plane is the Kelvin–Helmholtz instability wave. In addition to the supersonic instablity wave modes and the Kelvin–Helmholtz mode there are two families of zeros lying on the real k-axis; one to the left-hand branch point of η_o and the other to the right of the right-hand branch point of η_o. They are the subsonic wave modes. Some zeros remain in the upper half k-plane and some in the lower half plane. They represent spatially evanescent waves. It is to be noted that all the zeros of the dispersion function which originate from the upper half k-plane represent waves propagating in the downstream direction whereas those which originate from the lower half plane represent waves propagating in the upstream direction. When condition (2.13) is not satisfied, as in the case of a cold jet at 1.5 Mach number, there is no supersonic instability wave mode. In this case the trajectories of the zeros of $D(\omega, k)$ are shown in figure 11. In this figure only the zero of $D(\omega, k)$ corresponding to the Kelvin–Helmholtz instability wave crosses the real k-axis into the lower half plane. The subsonic wave zeros can be found along the real k-axis. But there is definitely no supersonic instability zero.

3.1. *Relationship between subsonic and supersonic wave modes*

In the previous section it was demonstrated that the Kelvin–Helmholtz instability wave is related to the supersonic instability waves. At high-jet Mach numbers the

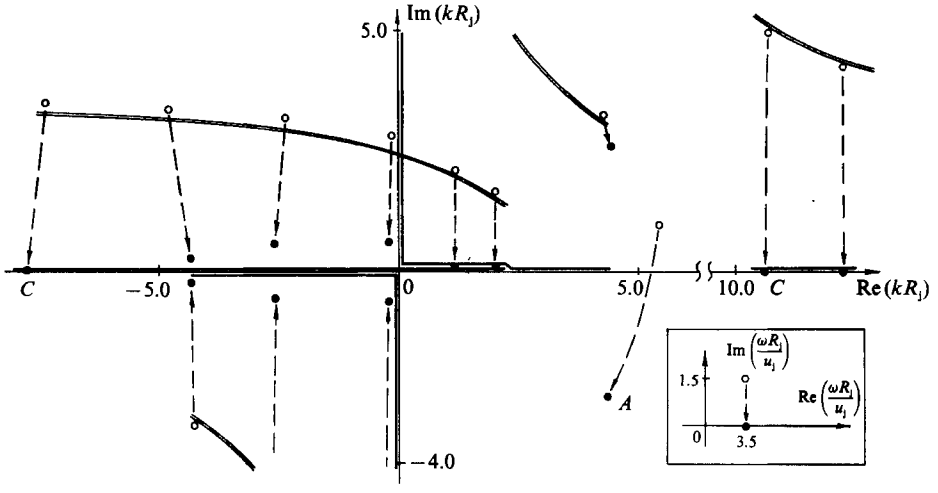

FIGURE 11. Trajectories of the zeros of $D(\omega, k)$ in the complex k-plane as $\mathrm{Im}\,(\omega) \to 0^+$ showing the Kelvin–Helmholtz instability wave (A) and the subsonic waves (C). Cold jet, Mach number 1.5, $n = 0$.

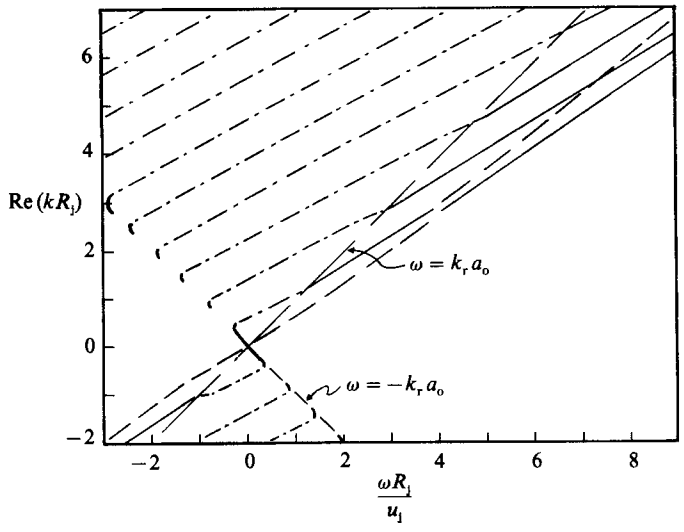

FIGURE 12. Dispersion relations, $\mathrm{Re}\,(k)$ as a function of ω, – – –, of the Kelvin–Helmholtz instability wave; ——, the supersonic instability waves; —·—·, The subsonic waves; and ——, the upstream propagating subsonic waves. Cold jet, jet Mach number 4.0, $n = 0$.

two sets of waves merge to form a single family. It turns out that the subsonic and supersonic waves, although seemingly different in that the former are neutral waves (in the context of the vortex-sheet model) while the latter are unstable waves, are also related. A clue to their relationship may be found in figure 10. For $\mathrm{Im}\,(\omega)$ large and positive the zeros of the supersonic instability waves and the subsonic waves form a family of zeros located near the right-hand branch cut of η_1. A more direct way of seeing that the two famlies of waves are related is to examine their dispersion relations. Figure 12 shows the relationship $k_r(\omega)$, where k_r is the real part of the axial wavenumber k, of the Kelvin–Helmholtz instability, the supersonic instability waves and the subsonic waves for a cold jet at Mach number 4.0. It is readily seen that the

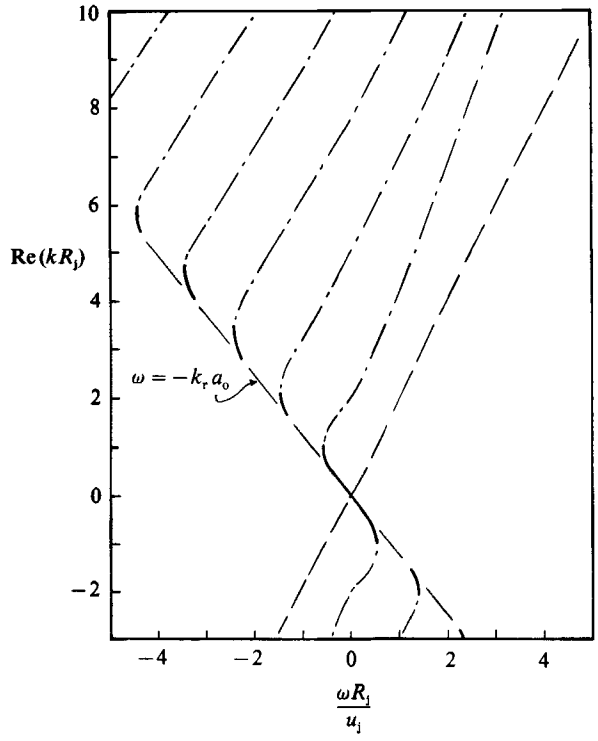

FIGURE 13. Dispersion relations, $k_r(\omega)$, of – – –, the Kelvin–Helmholtz instability wave; —·—·, the subsonic waves; ——, and the upstream propagating subsonic waves. Cold jet, Mach number 1.5, $n = 0$.

dispersion relations of the subsonic waves with positive k_r continue into the dispersion relations of the superonic instability waves. Thus they may technically be regarded as a single wave family exhibiting different characteristics in subsonic and supersonic convective Mach numbers.

At lower jet Mach number when condition (2.13) is not satisfied the supersonic instability waves do not exist. Figure 13 shows typical dispersion relations of the subsonic waves and the Kelvin–Helmholtz instability waves in this case. It is to be noted that the real part of the axial wavenumber, k_r, of the supersonic instability wave as well as that of the Kelvin–Helmholtz instability wave are smaller than those of the subsonic waves. This is evident in figure 10. This implies that the subsonic waves have the slowest phase velocities of the three families of waves. This result is consistent with the measurements of Oertel (1980).

3.2. *Upstream propagating waves of supersonic jets*

In a supersonic flow all small-amplitude disturbances propagate downstream. It is, therefore, natural to expect the intrinsic wave modes of a supersonic jet to propagate in the downstream direction. However, according to dispersion relation (2.7) a supersonic jet can support neutral upstream propagating wave modes. This finding is surprising but not unphysical. Outside the jet the ambient gas is stationary so it is possible for waves to propagate upstream but still be attached to the jet. The upstream propagating neutral waves, however, do not exist for all frequencies. Their existence is confined to very narrow frequency bands.

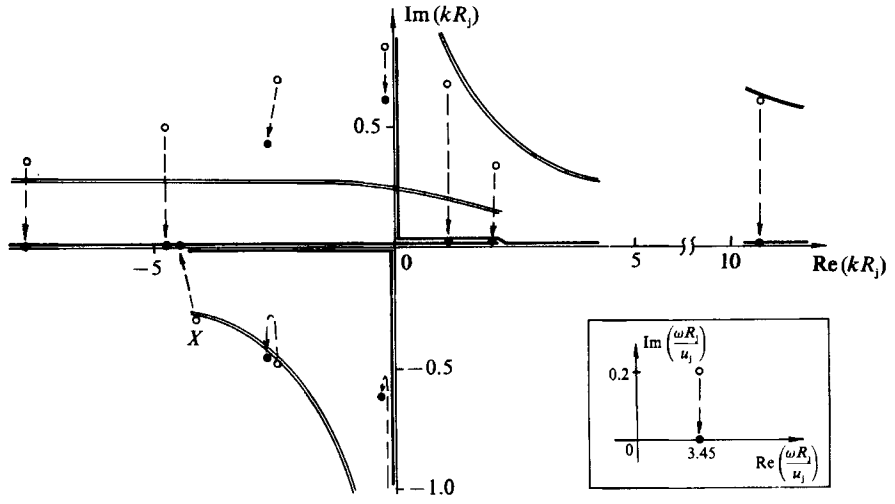

FIGURE 14. Trajectories of the zeros of $D(\omega, k)$ in the complex k-plane as $\mathrm{Im}\,(\omega) \to 0^+$ showing the upstream propagating subsonic wave marked by 'X'. Cold jet, Mach number 1.5, $n = 0$.

Experimentally it is known that supersonic jets operating at off-design condition normally would exhibit the phenomenon of screech during which strong discrete frequency sound waves are emitted. The screech is produced by a feedback loop (see Powell 1953; Davies & Oldfield 1962; Tam, Seiner & Yu 1986). Part of the feedback loop consists of strong acoustic disturbances propagating upstream immediately outside the jet toward the nozzle exit. It is not clear at this time whether these feedback acoustic disturbances of jet screech are associated with the upstream propagating wave modes found in this study or not.

To show the existence of upstream propagating wave modes for supersonic jets consider the trajectories of the zeros of the dispersion function $D(\omega, k)$ of (2.7) in the complex k-plane as shown in figure 14. In this figure the calculations are for a cold Mach 1.5 supersonic jet with $\mathrm{Re}\,(\omega R_j/u_j) = 3.45$. The trajectories are formed as ω is pushed from $\mathrm{Im}\,(\omega R_j/u_j) = 0.2$ to the real axis in the ω-plane according to Briggs' (1964) contour deformation criterion. As can be seen the trajectory X of the zero of $D(\omega, k)$ which begins in the lower half k-plane ultimately reaches the real k-axis when $\mathrm{Im}\,(\omega) \to 0^+$. Since this zero comes from the lower half plane it represents an upstream propagating neutral wave. Extensive numerical computation reveals that this zero reaches the real k-axis only for a narrow range of frequencies. At slightly higher frequencies this zero comes close to the real k-axis but remains in the lower half plane so that it is an upstream propagating evanescent wave. The spatial damping rate increases rapidly with frequency. Typical dispersion relations of the upstream propagating subsonic wave modes are shown in figure 13. The group velocity, $\partial\omega/\partial k_r$, is close to $-a_0$; a_0 is the ambient speed of sound. Hence in the (k_r, ω)-plane the dispersion relations of these waves lie very close to the straightline $\omega/k_r = -a_0$. Typical eigenfunctions of these waves will be given later.

3.3. *Wave pattern*

One way to identify the waves of high-speed jets predicted by the vortex-sheet or the finite shear-layer thickness jet models of §2 with those observed experimentally by Oertel (1980) is to compare the calculated and measured wave patterns. Consider the first two families of unstable waves, namely, the Kelvin–Helmholtz instability wave

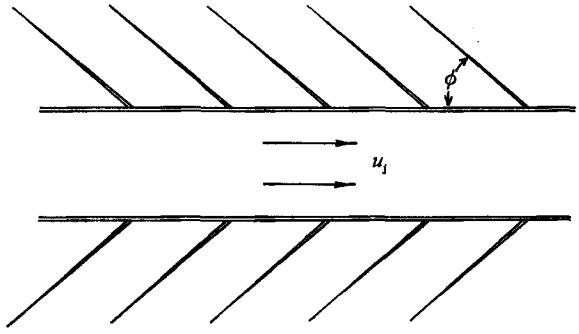

FIGURE 15. Lines of constant phase in the near field of a supersonic jet associated with the Kelvin–Helmholtz or supersonic instability waves.

and the supersonic instability waves. Outside the jet ($r > R_j$) the eigenfunction is given by (2.6) or

$$p_o(r,\theta,x,t) = AH_n^{(1)}(i\eta_o r)\, e^{i(kx+n\theta-\omega t)}, \tag{3.1}$$

where A is an arbitrary constant. For high-frequency waves, the wavelength is small compared to the diameter of the jet so that the argument of the Hankel function in (3.1) is large. It is, therefore, permissible to replace the Hankel function by its asymptotic form to obtain

$$\underset{r>R_j}{p_o(r,\theta,x,t)} \sim A\left(\frac{2}{i\pi\eta_o r}\right)^{\frac{1}{2}} \exp\{-\eta_o r + i[kx+n\theta-\omega t-\tfrac{1}{2}(n+\tfrac{1}{2})\pi]\}. \tag{3.2}$$

Here k and η_o are complex. Let

$$k = k_r + ik_i, \quad \eta_o = \eta_{or} + i\eta_{oi}. \tag{3.3}$$

Substitution of (3.3) into (3.2) leads to the following formula for p_o.

$$\underset{r>R_j}{p_o} \sim A\left(\frac{2}{i\pi\eta_o r}\right)^{\frac{1}{2}} \exp(-\eta_{or} r - k_i x)\exp\{i[-\eta_{oi} r + k_r x + n\theta - \omega t - \tfrac{1}{2}(n+\tfrac{1}{2})\pi]\}. \tag{3.4}$$

Consider a plane, θ = constant, which passes through the centreline of the jet. According to (3.4) on such a plane the curves of constant phase are straight lines. The equation of these lines is

$$k_r x - \eta_{oi} r - \omega t = \text{constant}. \tag{3.5}$$

This represents a set of parallel straight lines. These straight lines make an angle ϕ with the boundary of the jet as shown in figure 15. The angle ϕ is equal to

$$\phi = \tan^{-1}\left[\frac{k_r}{\eta_{oi}}\right]. \tag{3.6}$$

The wave pattern of figure 15 is the same as the wave pattern of the first set of waves in figure 1. In §4, (3.6) will be used to calculate the angle ϕ for the Kelvin–Helmholtz instability waves over a wide range of jet Mach number. There it will be shown that the calculated angles compared very favourably with experiments.

For supersonic instability waves the spatial growth rate is small. As a result η_{oi} is fairly small compared to k_r. ϕ as computed by (3.6) is, therefore, very close to 90°.

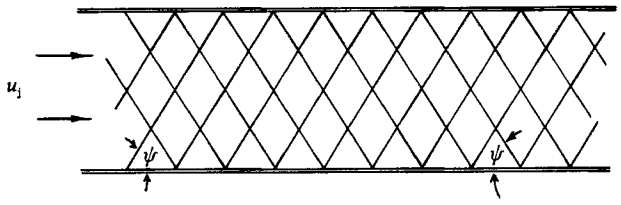

FIGURE 16. Lines of constant phase forming a cross-hatched pattern inside a supersonic jet associated with the subsonic waves.

This is consistent with the wavefront angle of the second set of waves shown in figure 1.

In the case of the neutral subsonic waves η_0 is real. Outside the jet the pressure distribution is given by

$$p_0 \underset{r>R_j}{\sim} A\left(\frac{2}{i\pi\eta_0 r}\right)^{\frac{1}{2}} \exp(-\eta_0 r)\exp[i(k_r x + n\theta - \omega t - \tfrac{1}{2}(n+\tfrac{1}{2}\pi))] \tag{3.7}$$

It is readily seen from (3.7) that the pressure distribution decays exponentially outward in the near field in all directions. In other words, the predicted wave pattern is confined inside the jet. This absence of a near-field wave pattern is the same as that of the third set of waves of figure 1.

Inside the jet pressure eigenfunction of the subsonic waves is given by (2.6). That is

$$p_i(r,\theta,x,t) \sim J_n(\eta_i r)\exp[i(kx + n\theta - \omega t)]. \tag{3.8}$$

For high-frequency waves $|\eta_i|r$ is large except near the jet axis. Under this circumstances one may again replace the Bessel function in (3.8) by its asymptotic form, hence

$$\begin{aligned} p_i(r,\theta,x,t) &\sim \frac{\text{constant}}{(\eta_i r)^{\frac{1}{2}}}\cos(\eta_i r - \tfrac{1}{2}(n+\tfrac{1}{2})\pi)\exp(i(kx+n\theta-\omega t)) \\ &\sim \frac{\text{constant}}{(\eta_i r)^{\frac{1}{2}}}[\exp(i(\eta_i r + kx + n\theta - \omega t - \tfrac{1}{2}(n+\tfrac{1}{2})\pi)) \\ &\quad + \exp(i(-\eta_i r + kx + n\theta - \omega t + \tfrac{1}{2}(n+\tfrac{1}{2}\pi))]. \end{aligned} \tag{3.9}$$

Now according to (3.9) the wave pattern in the plane θ = constant consists of two sets of propagating waves with curves of constant phase again in the form of parallel straight lines. The equations of the two families of straight lines are

$$\eta_i r + kx - \omega t = \text{constant}, \tag{3.10}$$

and

$$-\eta_i r + kx - \omega t = \text{constant}. \tag{3.11}$$

These two sets of parallel straight lines form a cross-hatched pattern inside the supersonic jet as shown in figure 16. The angle ψ between the straight lines and the jet boundary is given by

$$\psi = \tan^{-1}\left[\frac{k}{\eta_i}\right] = \sin^{-1}\left[\frac{a_j}{u_j - c_{ph}}\right], \tag{3.12}$$

where $c_{cp} = \omega/k$ is the phase velocity of the waves. This wave pattern is identical to that of the third set of waves observed by Oertel (1980) and labelled as the W'' waves in figure 1.

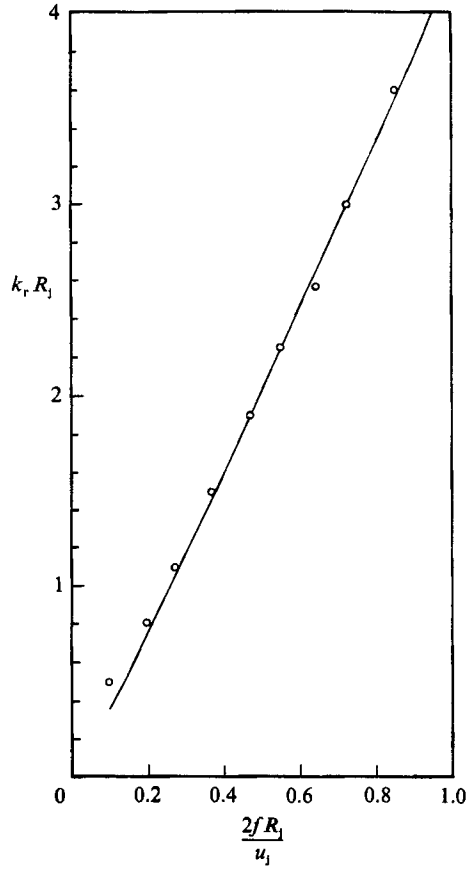

FIGURE 17. Comparison between calculated and measured dispersion relation of the Kelvin–Helmholtz instability wave in a cold 2.1 Mach number jet ($n = 1$). ——, calculated; O, experiment of Troutt & McLaughlin (1982).

The identification of the wave patterns of the three sets of waves observed by Oertel as the Kelvin–Helmholtz instability wave, the supersonic instability waves and the subsonic waves found in the present analysis is now complete. In the following sections special characteristics of each set of waves will be discussed. Comparisons with experiments will be made whenever possible.

4. Wave pattern and other characteristics of Kelvin–Helmholtz instability

The Kelvin–Helmholtz instability wave has been studied by numerous investigators before. Michalke (1984) has provided an excellent review of this instability in subsonic jets. Here only the important features of this instability wave in supersonic jets will be presented. Emphasis will be on comparisons with experiments. Some of the characteristic features of the Kelvin–Helmholtz waves will also be described. This is for the purpose of providing a basis for comparison with the supersonic instability waves in the next section.

Measurements of pressure and velocity disturbances in supersonic flows are difficult to perform. As a result there is only a limited number of experiments on Kelvin–Helmholtz instability waves in supersonic jets. By comparing the calculated

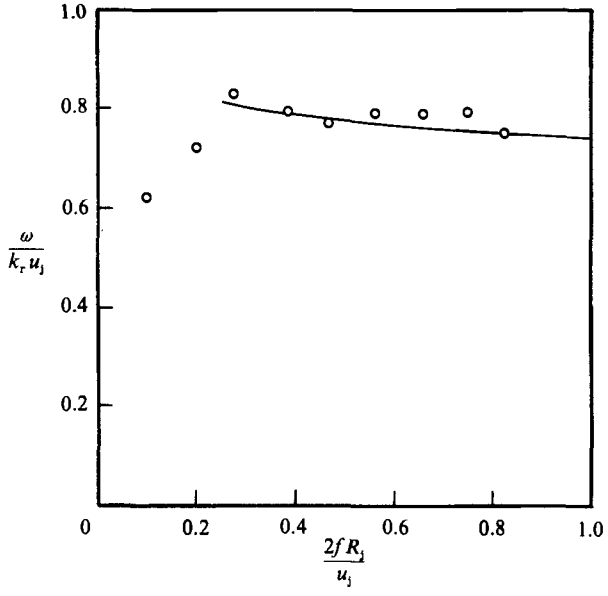

FIGURE 18. Comparison between calculated and measured wave speed of the Kelvin–Helmholtz instability wave in a cold 2.1 Mach number jet ($n = 1$). ——, calculated; ○, experiment of Troutt & McLaughlin (1982).

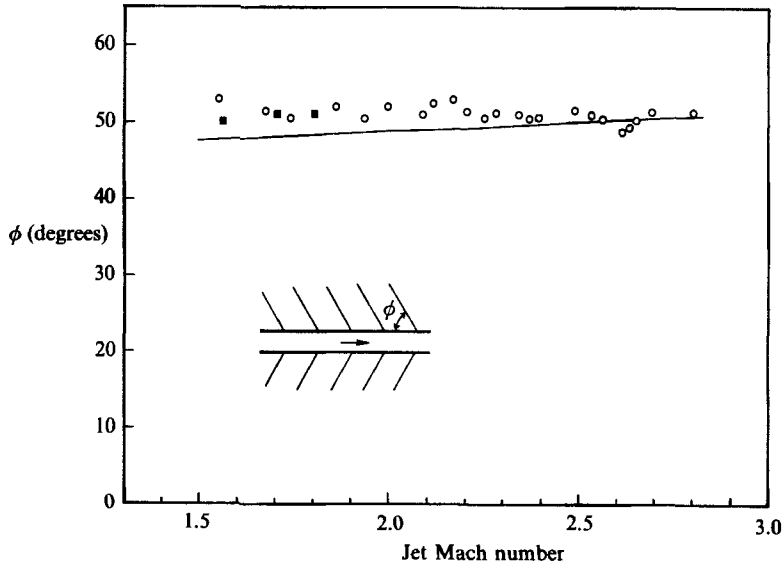

FIGURE 19. Comparison between calculated and observed angle of the wavefronts of the Kelvin–Helmholtz instability waves outside a supersonic nitrogen jet. ——, calculation (high frequency); experiment: ○, Rosales (1970); ■, Lowson & Ollerhead (1968).

results with these measurements it appears that linear stability theory can provide reasonably good estimates of the wave speed and near-field pattern. However, the calculated growth rate is quite inaccurate. This situation is similar to that for subsonic jets as reported by Moore (1977) and others. Figure 17 shows the calculated dispersion relation of the Kelvin–Helmholtz instability wave (equation (2.7)) for a

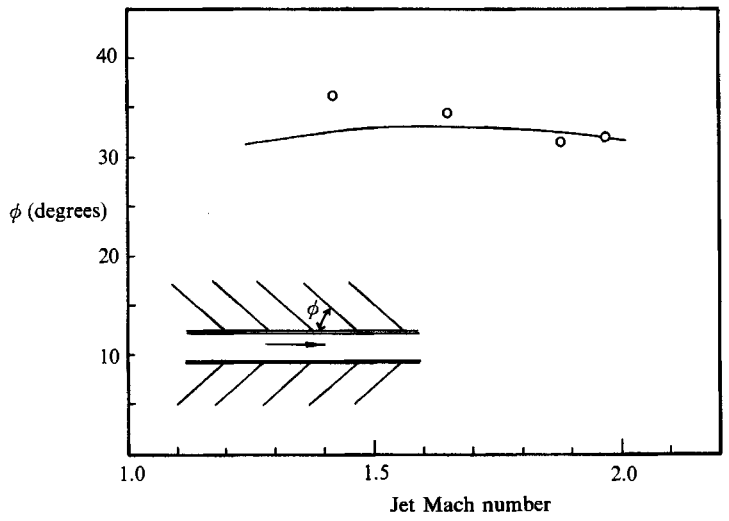

FIGURE 20. Comparison between calculated and observed angle of the wavefronts of the Kelvin–Helmholtz instability waves outside a supersonic helium jet. ——, calculation (high frequency); ○, experiment of Rosales (1970).

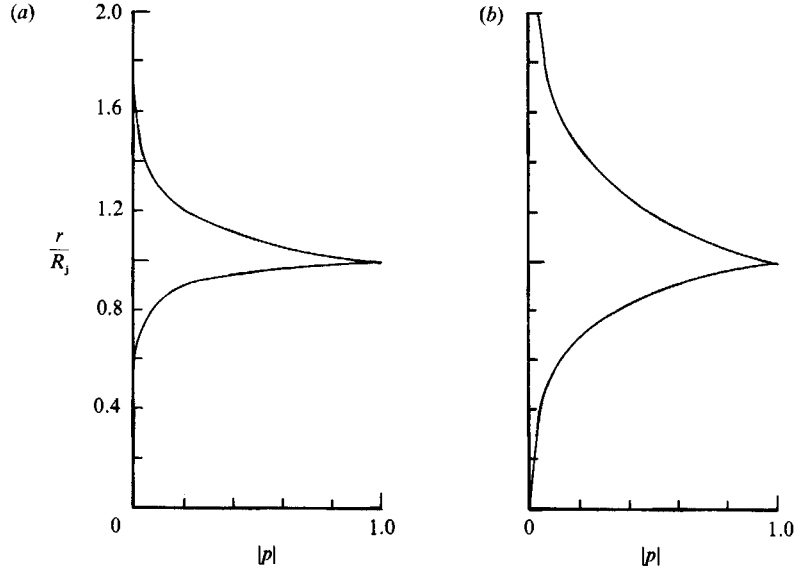

FIGURE 21. Pressure eigenfunction distribution of the Kelvin–Helmholtz instability waves. Mach 1.6 cold jet, axisymmetric mode ($n = 0$). (*a*) $\omega R_j/a_o = 11.0$, (*b*) 5.0.

2.1 Mach number cold jet for the $n = 1$ wave mode. Plotted in this figure also are the measurements of Troutt & McLaughlin (1982). Figure 18 shows a comparison of the calculated and measured wave speed over the Strouhal number range of 0.1–0.9. As can be seen there is good agreement between theory and experiment over nearly the whole range of Strouhal number.

Prior to the work of Oertel (1979), Lowson & Ollerhead (1968) and Rosales (1970) had carried out extensive observations of the near-field wave pattern of the

Kelvin–Helmholtz instability waves in supersonic jets. These data can now be used to compare with the calculated wave pattern discussed in §3.3. Figure 19 shows the observed wave-front angle of cold supersonic nitrogen jets as a function of jet Mach number. The full curve in this figure is the calculated angle based on (3.6) at high frequency. The agreement with measurements is excellent. The difference between theoretical values and measurements is well within expected experimental uncertainty. Figure 20 is a similar comparison between calculated and observed wave-front angles for supersonic helium jets. Because of the not insignificant difference in the ratio of specific heats of the gas inside and outside the jet the wave-front angle reduces greatly from figure 19 to figure 20. This is correctly calculated by (3.6). The good agreements found between theory and experiment tend to reinforce the belief that the near wave field of the first set of waves observed by Oertel (1980) is indeed associated with the Kelvin–Helmholtz instability wave.

Figure 21 shows the pressure eigenfunction associated with the Kelvin–Helmholtz instability wave in a cold Mach number 1.6 supersonic jet. It is evident from this figure that the pressure fluctuations are confined to the region immediately adjacent to the shear layer of the jet. There is very little pressure fluctuation near the jet centreline. The instability wave distribution is similar to that of a plane two-dimensional shear layer. The axisymmetric geometry of the jet mixing layer seems to be unimportant. This is in sharp contrast to the supersonic instability waves which owe their existence to nearly complete reflection of acoustic disturbances at the shear layer of the jet.

5. Characteristics of supersonic instability waves

As discussed in §1, supersonic instability waves are sustained by continuous reflection of acoustic disturbances at the mixing layer of the jet. The entire wave family consists of infinitely many modes. These wave modes can be classified by designating each mode by two integer numbers (n, m). The n number is the azimuthal mode number from the $\exp(in\theta)$ $(n = 0, 1, 2, \ldots)$ dependence of the wave solution. The m number $(m = 1, 2, 3, \ldots)$ is the radial mode number characterizing the number of anti-nodes (maximum oscillation points) of the presure distribution of the wave in the radial direction. As an illustration figures 22 and 23 show the pressure eigenfunction distribution of the (0, 1), (0, 2), (0, 3), (1, 1), (1, 2) and (1, 3) supersonic instability wave modes of a cold Mach number 3.0 jet. The number of antinodes is well defined so that the m number assigned to a mode is unambiguous. For all axisymmetric modes $(n = 0)$ the first antinode is located at the centre of the jet. On the other hand for the higher-order modes $(n = 1, 2, 3, \ldots)$ the centre of the jet is a node as shown in figure 23. It is interesting to compare the pressure eigenfunctions of figures 22 and 23 with those of the Kelvin–Helmholtz instability wave shown in figure 21. The antinodes and quasi-nodes (minimum oscillation points) of the eigenfunctions of supersonic instability waves are characteristics of waves generated by continuous reflection. There are no such features in the eigenfunctions of the Kelvin–Helmholtz instability waves. The distinct differences between figures 21 and 22 or 23 reflect simply the different physical mechanisms which drive these two familes of instabilities.

Typical dispersion relations, $\mathrm{Re}(k)$ as a function of ω, of the supersonic instability waves are shown in figure 12. Once the dispersion relation of a wave mode is known the phase velocity $c_{\mathrm{ph}} = \omega/\mathrm{Re}(k)$ can easily be determined. The spatial growth rate of a supersonic instability wave varies with the frequency of the wave. Figure 24

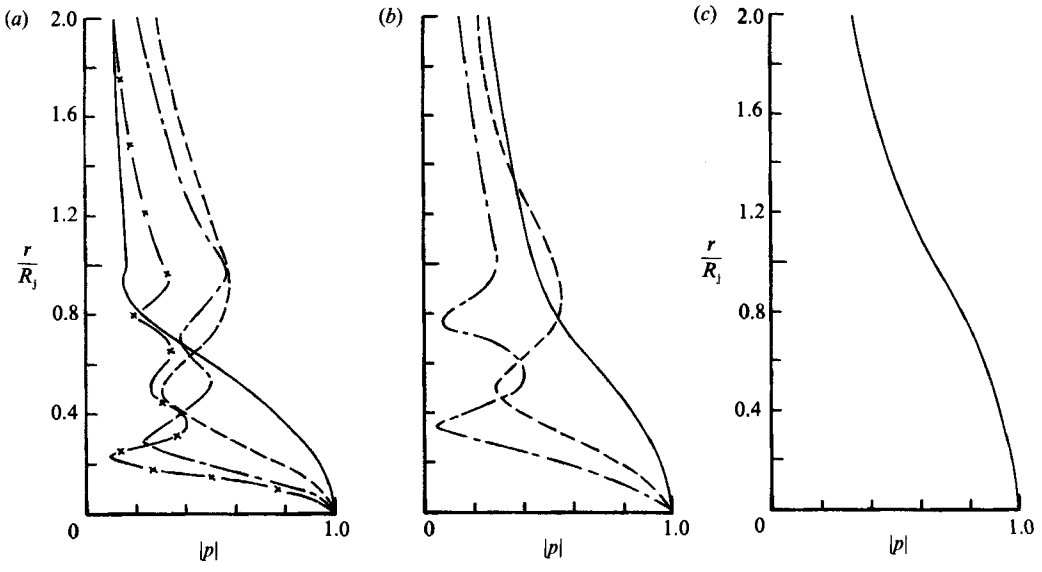

FIGURE 22. Pressure eigenfunction distributions of supersonic instability waves. Cold jet, Mach number 3.0. ——, (0, 1) mode; – – –, (0, 2) mode; — · — · —, (0, 3) mode; — × — × —, (0, 4) mode. (*a*) $\omega R_j/a_0 = 16.0$, (*b*) 8.5, (*c*) 2.0.

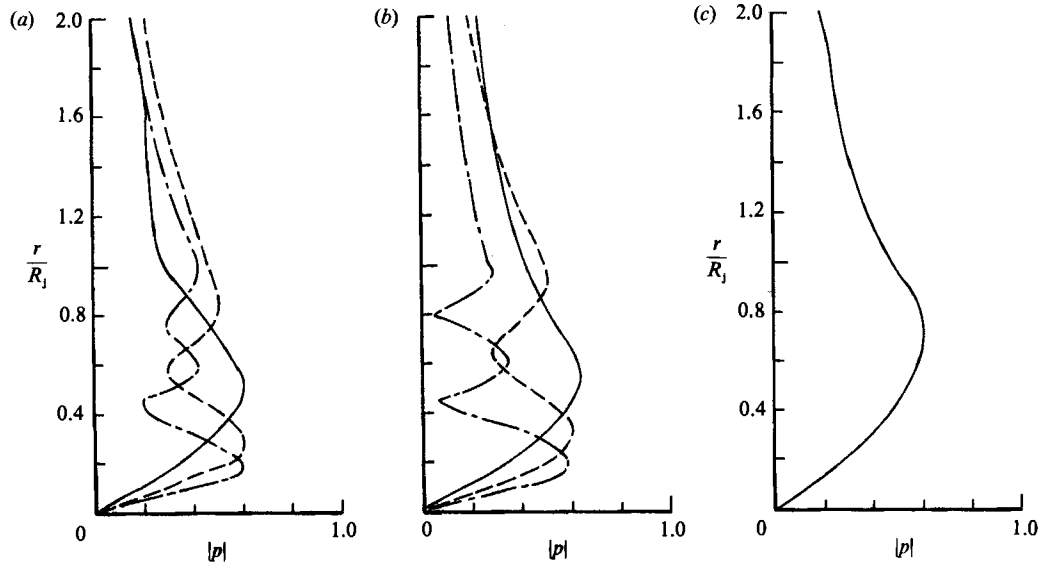

FIGURE 23. Pressure eigenfunction distributions of supersonic instability waves. Cold jet, Mach number 3.0. ——, (1, 1) mode; – – –, (1, 2) mode; — · — · —, (1, 3) mode. (*a*) $\omega R_j/a_0 = 16.1$, (*b*) 10.1, (*c*) 3.0.

provides the spatial growth rates of the first six axisymmetric modes ($n = 0, m = 1, 2, 3, \ldots, 6$) of a cold Mach number 4.0. These waves are typical of the entire family of supersonic instability waves. Each wave mode is unstable over a certain frequency band and attains maximum growth rate at a particular frequency. In figure 24 the most unstable frequencies for the first five radial modes, i.e. $m = 1, 2, 3, 4, 5$, are

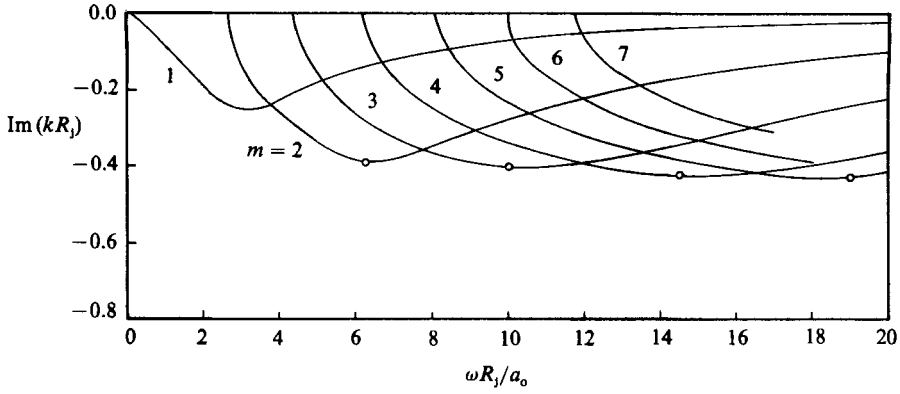

FIGURE 24. Spatial growth rate of supersonic instability waves. Cold jet, Mach number 4.0, axisymmetric mode ($n = 0$). ○, maximum growth rate of the wave mode.

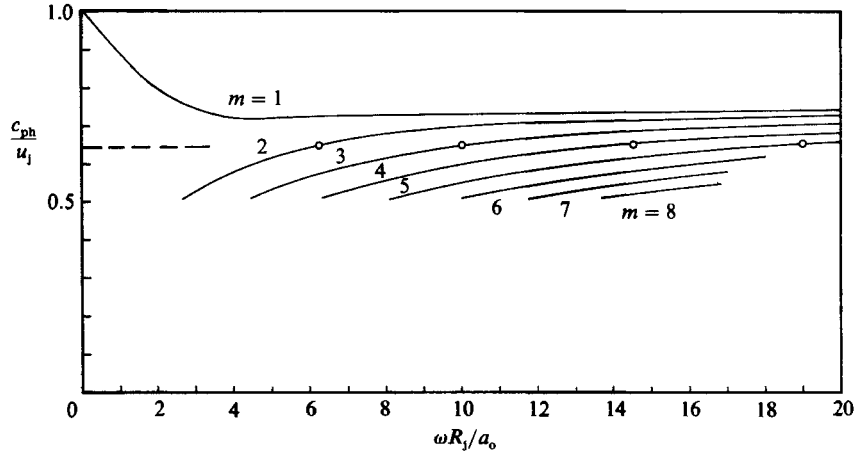

FIGURE 25. Phase velocities of supersonic instabilty waves. Cold jet, Mach number 4.0, axisymmetric mode ($n = 0$). ○, wave with maximum spatial growth rate; – – –, most probable wave speed.

denoted by a circle. The phase velocities corresponding to the waves of figure 24 are shown in figure 25 as functions of $\omega R_j/a_o$. The phase speeds of the wave of each mode with maximum spatial growth rates are indicated by circles. It is important to observe that the phase velocities of the most amplified wave of various modes are nearly equal. The averaged numerical value is indicated by the dotted line in the figure. Since this is the phase velocity of the most amplified wave it is, therefore, the most likely observed wave speed. As suggested by figure 25 this wave speed is largely independent of frequency, jet radius and radial mode number m. It turns out that it is also independent of the azimuthal mode number n and jet Mach number. Extensive numerical computations have been carried out to determine the parameter which would correlate with this calculated most probable wave speed. It has been found that this wave speed is a function of jet to ambient speed of sound. The parameter which correlates with all the computed results is $(1+a_j/a_o)^{-1}$; assuming that the specific heat ratios inside and outside the jet are the same. Figure 26 shows that the calculated most probable wave speed of the supersonic instability waves is

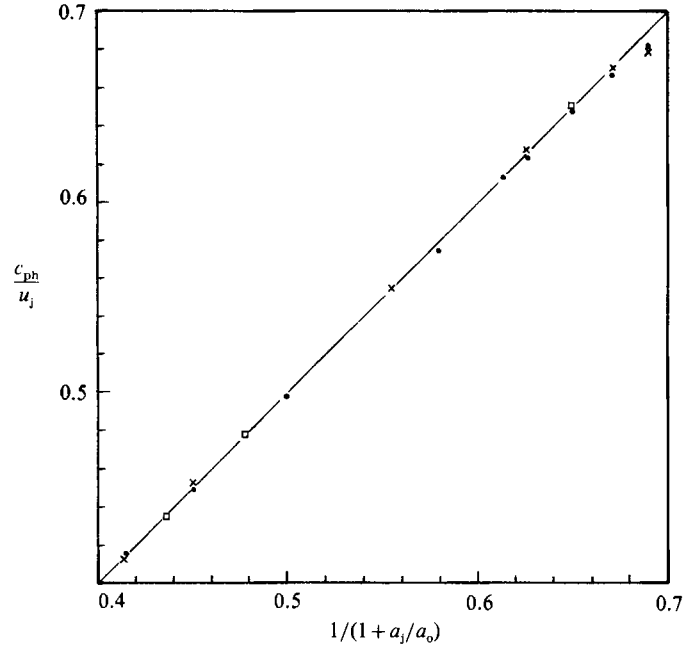

FIGURE 26. Correlation of the phase velocity of supersonic instability wave at maximum spatial growth rate with the parameter $[1+a_j/a_o]^{-1}$. ●, $n=0$; ×, $n=1$; □, $n=2$ ($\gamma_j=\gamma_o$).

directly proportional to this parameter. Since the computed points lie almost exactly on the 45° line it is concluded that the most likely observed phase velocity, c_{ph}, of the supersonic instability waves is given by the formula

$$\frac{c_{ph}}{u_j}=\frac{1}{1+a_j/a_o}. \tag{5.1}$$

Equation (5.1) is identical to an empirical formula derived by Oertel (1980) based on his extensive experimental measurements. It correlates a large body of his measured data. The perfect agreement between calculated results and experiments leaves little room for doubt that the second set of waves (see figure 1) observed by Oertel are, indeed, the supersonic instability waves. It is worth mentioning that Papamoschou & Roshko (1986) in their study of large turbulence structures in high-speed two-dimensional shear layers derived an equation identical to (5.1) using simple quasi-steady flow argument. It appears, therefore, that (5.1) might be applicable even to disturbances of moderately large amplitude.

Equation (5.1) is independent of the radius of the jet. By using this information it is possible to derive this equation from the dispersion relation (2.7). Since the most probable wave speed is independent of jet radius R_j, one can let $R_j k\to\infty$ in (2.7). In this limit the entire family of the supesonic instability waves reduces to a single neutral wave. If the ratio of the specific heats of the gas of the jet, γ_j, differs only slightly from that of the ambient gas, γ_o, i.e. $(\gamma_j/\gamma_o-1)\ll 1$ then it is straightforward to show that the phase speed of the limiting neutral wave, to order $(\gamma_j/\gamma_o-1)^2$, is

$$\frac{c_{ph}}{u_j}=\frac{1}{1+a_j/a_o}+\left(\frac{\gamma_j}{\gamma_o}-1\right)\frac{a_j a_o[u_j^2-(a_j+a_o)^2]}{(a_j+a_o)^2[u_j^2-2(a_j+a_o)^2]}. \tag{5.2}$$

When γ_j and γ_o are equal, (5.2) reduces to (5.1).

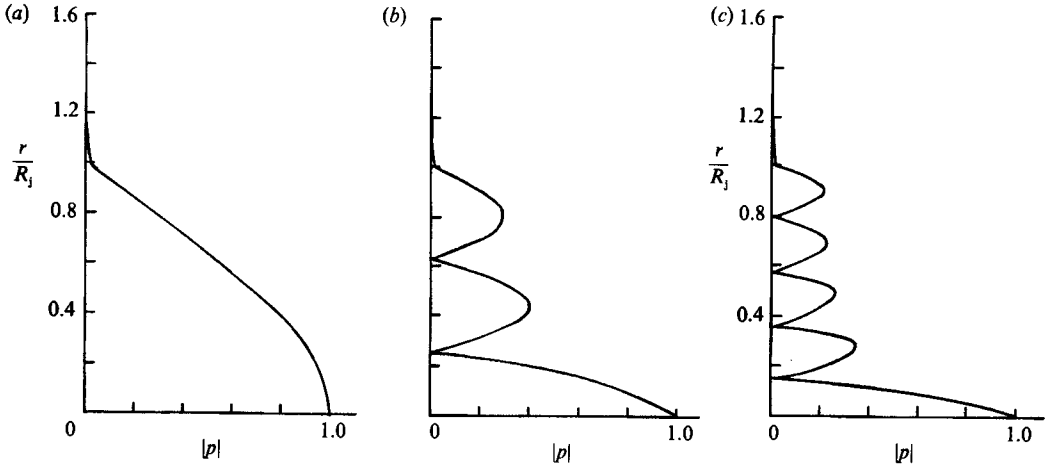

FIGURE 27. Pressure eigenfunctions of subsonic waves. Cold jet, Mach number 1.5, $kR_j = 15.0$. (*a*) (0, 1) mode, (*b*) (0, 3) mode, (*c*) (0, 5) mode.

6. Characteristics of subsonic waves

As has been pointed out in §3, at high frequencies the subsonic waves continues into the supersonic instability waves. The major differences between these two families of waves are that the former are neutral waves (within the framework of the vortex-sheet jet model) with subsonic phase velocities relative to the ambient gas while the latter are spatially amplifying waves travelling with supersonic phase velocities. In addition, supersonic instability waves exist only when condition (2.13) is satisfied. On the other hand subsonic waves exist regardless of the jet Mach number and velocity. As in the case of supersonic instability waves, subsonic waves can be classified into modes by two integers (n, m). Again n is the azimuthal wavenumber and m is the radial wavenumber which is equal to the number of antinodes the pressure eigenfunction has. Figure 27 shows the pressure eigenfunction of the (0, 1), (0, 3) and (0, 5) subsonic wave modes of a cold Mach number 1.5 jet at $kR_j = 15.0$. The antinodes are well defined so that no ambiguity could arise in assigning the m numbers. The eigenfunction distributions in figure 27 are typical of this entire family of waves. The disturbance decays quickly in the radial direction outside the jet so that the waves are essentially confined inside the jet flow. This is in complete agreement with the third set of waves observed by Oertel (1980), see figure 1.

Subsonic waves exist in subsonic as well as in supersonic jets. One important difference being that for a given frequency there is only a finite number of subsonic modes in a subsonic jet whereas there are infinitely many such wave modes in a supersonic jet. As an illustration, figure 28 provides the dispersion relations of these waves for a subsonic jet of Mach number 0.6. For subsonic jets all the waves of this wave family propagate upstream. There is no downstream propagating subsonic waves. Being upstream propagating waves, they have negative group velocities. In other words, the slopes of the dispersion relations of figure 28 are negative. For supersonic jets there are upstream as well as downstream propagating subsonic waves. This point was discussed in §3 using the complex k-plane. Another way of seeing the existence of both upstream and downstream propagating subsonic waves

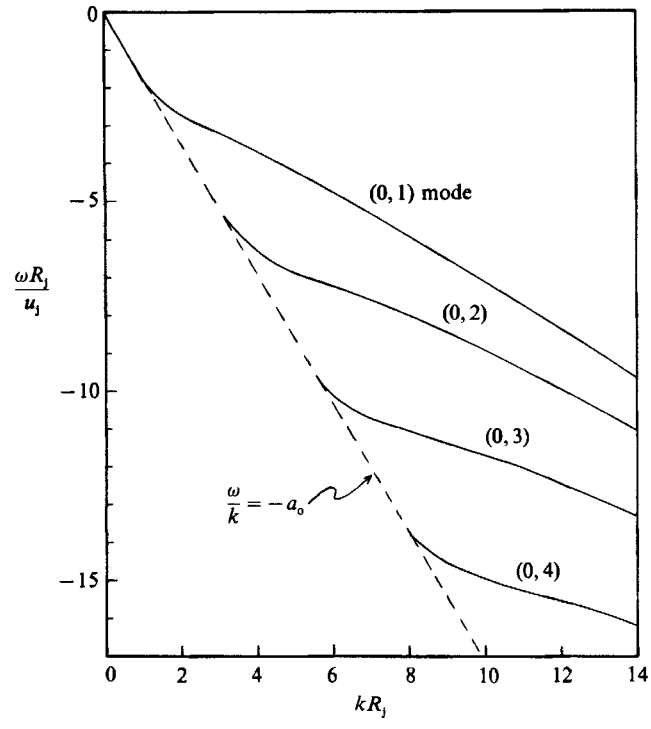

FIGURE 28. Dispersion relations of subsonic waves for a cold Mach number 0.6 jet. All waves propagate upstream.

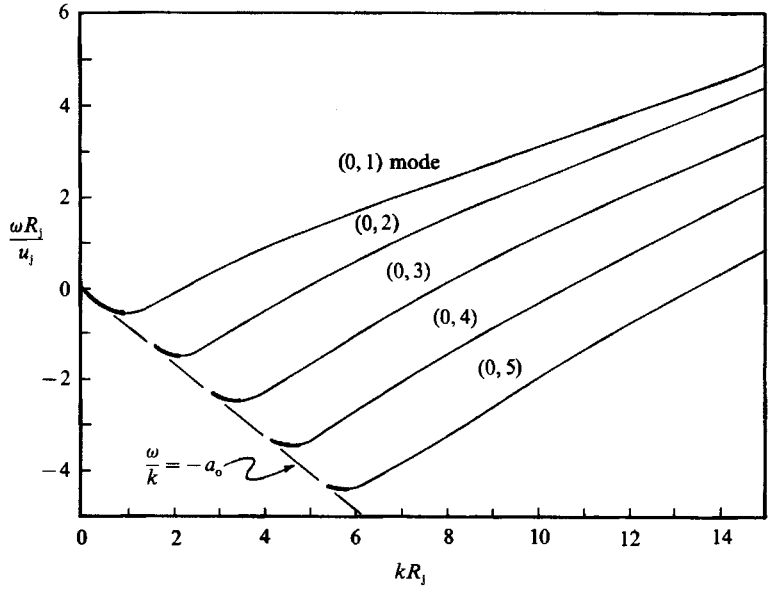

FIGURE 29. Dispersion relations of subsonic waves for a cold Mach number 1.5 jet. ——, upstream propagating waves; ——, downstream propagating waves; axisymmetric mode ($n = 0$).

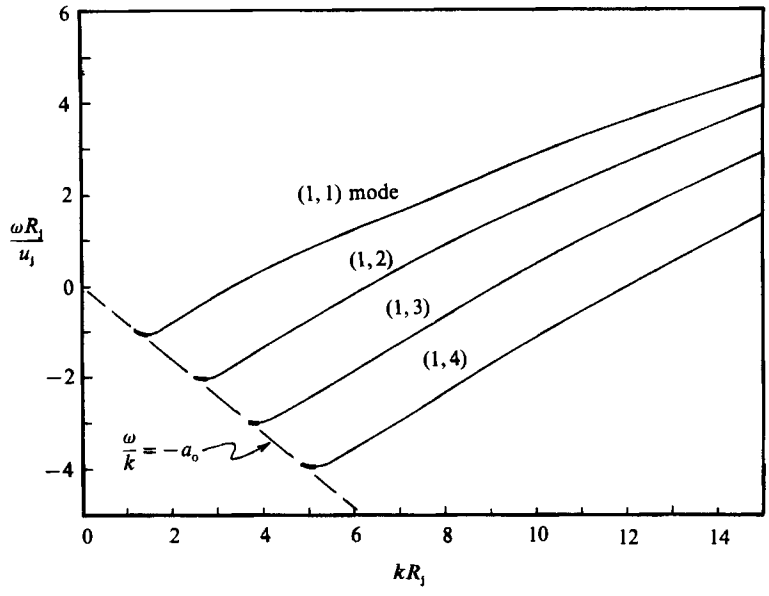

FIGURE 30. Dispersion relations of subsonic waves for a cold Mach number 1.5 jet. ——, upstream propagating waves; ——, downstream propagating waves; helical mode ($n = 1$).

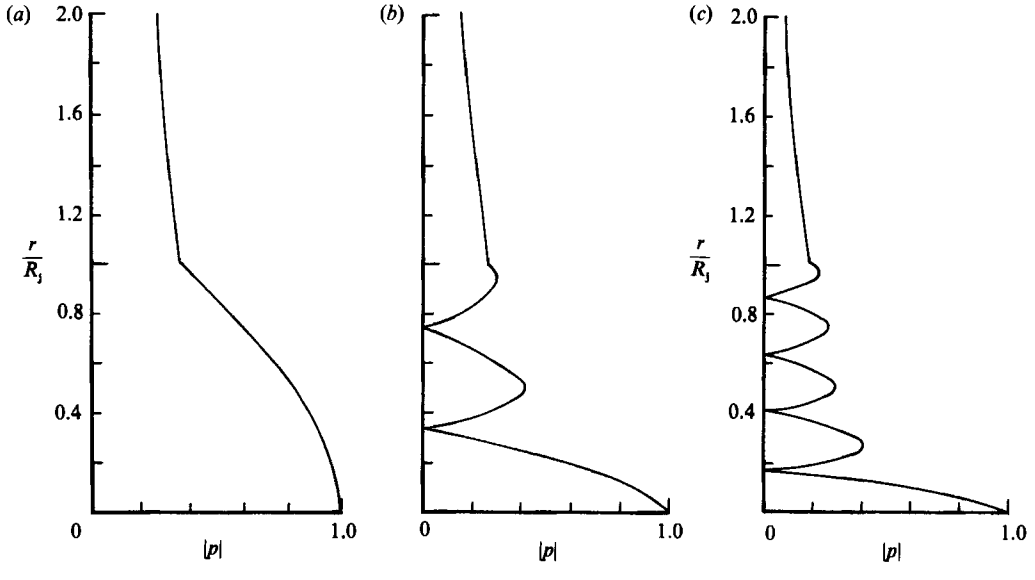

FIGURE 31. Pressure eigenfunctions of upstream propagating subsonic waves. Cold jet, Mach number 1.5. (*a*) (0, 1) mode, $kR_j = 0.7$, (*b*) (0, 3) mode, $kR_j = 3.0$, (*c*) (0, 5) mode, $kR_j = 5.5$

is to examine their dispersion relation. Figures 29 and 30 are typical dispersion relations of these waves for a supersonic jet. For each wave mode the dispersion relation exhibits a minimum slightly to the right of the line $\omega/k = -a_0$. To the left of the minimum the waves have negative group velocities and, therefore, propagate upstream. To the right of the minimum the slope of the curve or group velocity is positive. Hence these waves propagate in the same direction as the jet flow. At the

minimum point the two wave modes coalesce. In other words there is a double zero in the k-plane. For frequencies lower than the minimum the double zero moves off the real k-axis to become a complex conjugate pair. They are, therefore, spatially evanescent waves propagating in opposite directions.

For supersonic jets the range of frequencies over which upstream propagating subsonic waves are possible is restricted to narrow frequency band, see figures 29 and 30. In these figures it is observed that the dispersion relations of these waves lie very close to the line $\omega/k = -a_0$. Thus the phase speeds of these waves are equal to $-a_0$. Figure 31 shows the pressure eigenfunctions associated with the upstream propagating subsonic waves. One important characteristic difference between these eigenfunctions and those of the downstream propagating waves, see figure 27, is that they extend well outside the jet flow. This is, of course, necessary, for unless the main part of the wave propagates outside the jet it would be swept downstream by the supersonic jet flow. The dispersion relations of upstream propagating subsonic waves terminate on the line $\omega/k = -a_0$. The limiting behaviour of the dispersion relation at this line can be found directly from (2.7). In the limit $\omega/k \to -a_0, \eta_0$ of (2.7) goes to zero. By means of the asymptotic formula for Hankel functions with small argument it is easy to show that (2.7) becomes, in the case of $n = 0$,

$$\frac{J_0(\eta_i R_j)}{kR_j \ln(\eta_0 R_j)} + \frac{\rho_0}{\rho_j} \frac{[(a_0/a_j + M_j)^2 - 1]^{\frac{1}{2}}}{(a_0/a_j + M_j)^2} \left(\frac{a_0}{a_j}\right)^2 J_1(\eta_i R_j) = 0, \tag{6.1}$$

where $M_j = u_j/a_j$ is the jet Mach number.

There are two types of solution to (6.1)

(*a*) $\omega/k \to -a_0, k \neq 0$. This corresponds to the $(0, m), m = 2, 3, 4, \ldots$, subsonic wave modes. In this case (6.1) reduces to

$$J_1(\eta_i R_j) = 0, \tag{6.2}$$

so that $\eta_i R_j = \sigma_{m-1} (m = 2, 3, 4, \ldots)$ where σ_{m-1} are the zeros of J_1. From this relationship it is straightforward to find the limiting frequencies to be

$$\lim_{\omega/k \to -a_0} \frac{\omega R_j}{u_j} \to \frac{-\sigma_{m-1} k/|k|}{M_j \frac{a_j}{a_0} \left[\left(\frac{a_0}{a_j} + M_j\right)^2 - 1\right]^{\frac{1}{2}}}, \quad (m = 2, 3, 4, \ldots). \tag{6.3}$$

These limiting frequencies are the starting point of the dispersion curves in figure 29.

(*b*) $\omega/k \to -a_0, k \to 0$ simultaneously. This corresponds to the $(0, 1)$ subsonic wave mode. In this special case the solution of (6.1) has the form

$$\omega/k \to -a_0 + \beta e^{-\mu/k^2}, \tag{6.4}$$

where β and μ are positive real constants. This form of the solution makes the term $k \ln(\eta_0 R_j) \to$ finite instead of infinite as $\omega/k \to -a_0$ in (6.1). For this particular solution the dispersion relation passes through the origin as shown in figure 29. It is to be noted that such a special solution does not exist for non-axisymmetric modes.

For $n \neq 0$, (2.7) in the limit $\omega/k \to -a_0$ reduces to

$$nJ_n(\eta_i R_j) + \frac{\rho_0}{\rho_j} \frac{a_0^2 \eta_i R_j}{(a_0 + u_j)^2} J'_n(\eta_i R_j) = 0, \tag{6.5}$$

this equation determines the limiting value of $\eta_i R_j$ from which the limiting

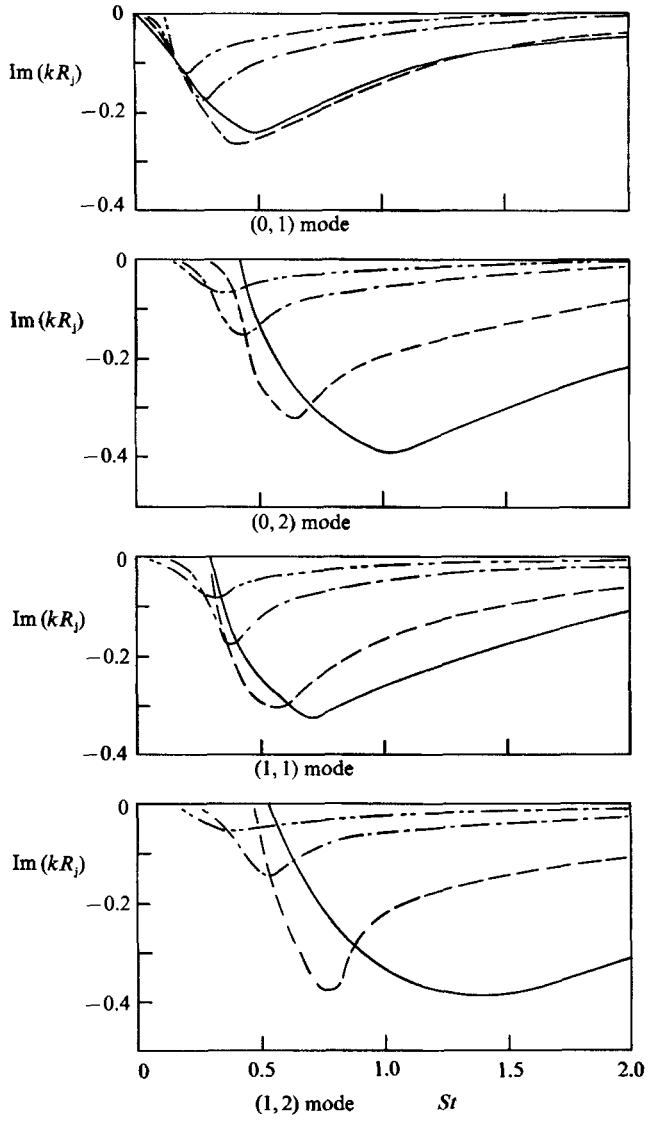

FIGURE 32. Spatial growth rates of supersonic instability waves as functions of Strouhal number. ——, $b/R_j = 0$; – – –, $b/R_j = 0.02$; — · — · —, $b/R_j = 0.1$; — · · — · · —, $b/R_j = 0.2$. Cold jet, Mach number 4.0. $St = 2fR_j/u_j$.

frequencies can be easily found. These limiting frequencies are shown as the starting points of the dispersion curves in figure 30.

7. Jets with finite thickness mixing layer

In Oertel's experiments the shock-tube facility was able to produce jets with relatively thin mixing layers so that a vortex-sheet jet model is a good first approximation. To investigate the effects of finite mixing-layer thickness on the three families of waves the jet model of §2.2 is used. For the Kelvin–Helmholtz instability waves the finite thickness effects are well known. At a fixed Strouhal

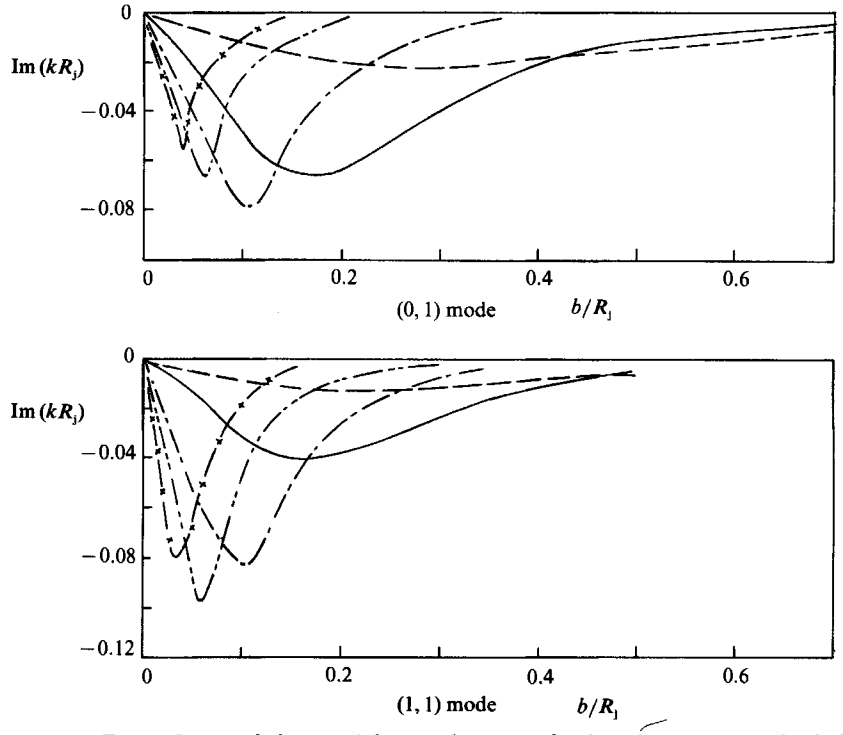

FIGURE 33. Dependence of the spatial growth rates of subsonic waves on the half-width of the mixing layer of a cold Mach number 2.0 jet at different Strouhal numbers. – – –, $St = 0.2$; ——, $St = 0.4$; — · — · —, $St = 0.8$; — · · — · · —, $St = 1.2$; — × — × —, $St = 1.6$.

number the spatial growth rate of the wave decreases with increase in mixing-layer thickness. The wave speed is, however, only slightly affected by shear-layer thickness. In this section, therefore, attention will be focused mainly on the supersonic and subsonic waves.

According to the vortex-sheet model the supersonic waves of a high-speed jet are unstable. It turns out that by increasing the thickness of the shear layer of the jet the maximum spatial growth rate of each mode would generally be reduced. Figure 32 shows the change in the spatial growth rates of these waves in a Mach 4.0 cold jet as the half width of the shear layer increases. As can be seen the change depends on the wave mode and the Strouhal number. For jets with thicker mixing layers the maximum growth rate occurs at lower Strouhal number. In fact, the spatial growth rate at the low-frequency range may actually increase. On the other hand the growth rates of high-frequency waves do decrease with increase in mixing-layer thickness. Another interesting observation of figure 32 is that for jets with thin mixing layers the higher-order modes (both higher azimuthal and or radial mode number) have larger growth rates. Whereas for jets with realistic thickness the growth rates of the lower-order supersonic modes tend to be relatively larger, although they are smaller in an absolute sense. Unlike spatial growth rates, extensive numerical computations indicate that the phase velocities of supersonic instability waves are almost unaffected by mixing-layer thickness. This behaviour is similar to the Kelvin–Helmholtz instability waves. Thus as long as the jet mixing layer is fairly thin the phase velocity formulae of (5.1) and (5.2) are applicable.

The effects of finite mixing-layer thickness on the subsonic waves of a high-speed

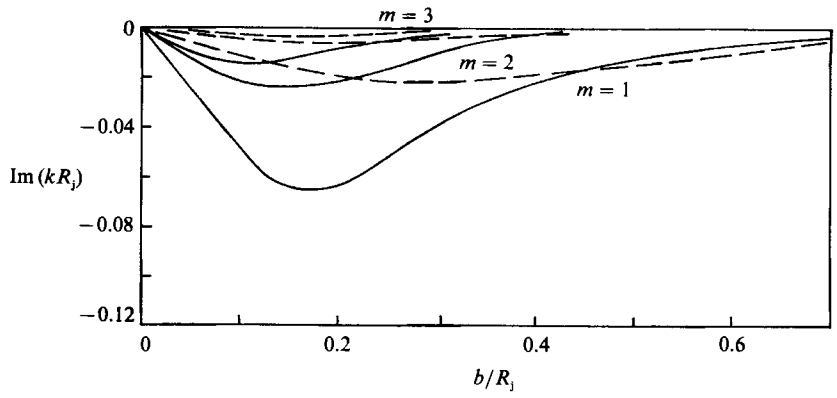

FIGURE 34. Effect of radial mode numbers on the growth rate of subsonic instability waves. Cold jet, Mach number 2.0, axisymmetric modes. ——, $St = 0.4$; – – –, $St = 0.2$.

jet are quite unusual and unexpected. For supersonic jets with zero-thickness mixing layers the vortex-sheet model suggests that they are neutral waves. However, calculations based on the finite shear-layer thickness jet model of §2.2 reveal that the downstream propagating modes are unstable waves. Figure 33 shows the spatial growth rates of a few of the low-order subsonic wave modes of a Mach 2.0 cold jet at several Strouhal numbers as functions of mixing-layer thickness. At a fixed Strouhal number a subsonic wave is unstable over a range of thicknesses. However, unlike the Kelvin–Helmholtz or the supersonic instability waves the maximum spatial growth rate does not occur at zero thickness. Instead, for each frequency there is an optimal thickness for maximum growth. Figure 34 provides basic information regarding the dependence of the growth rate on radial mode number. It is clear from this figure that higher-order radial wave modes tend to be less unstable. The same is true for higher-order azimuthal mode number. In other words, the low-order modes are the most unstable and hence they are most likely to be observed in experiments.

Numerical studies indicate that the phase velocity of a subsonic wave is unaffected by the thickness of the shear layer over the range of b/R_j up to 0.5. This aspect of the subsonic waves is similar to that of the Kelvin–Helmholtz and the supersonic instability waves. For upstream propagating subsonic waves of supersonic jets the present investigation indicates little or no finite mixing-layer-thickness effect. The waves appear to remain neutral. The reason why finite mixing-layer thickness has different effects on upstream and downstream propagating waves is not clear. Although one major difference between upstream and downstream propagating waves is that the former has no critical layer whereas the latter does. However, whether this is, indeed, the reason for the absence of finite mixing-layer-thickness effect on upstream propagating subsonic waves remains an open question at this time.

8. Summary of numerical results

Extensive computations on the growth rates and propagation characteristics of the Kelvin–Helmholtz, the supersonic and the subsonic instability waves at various jet Mach numbers, jet to ambient temperature ratios and mixing-layer thicknesses have been carried out. Here the essence of these different results will be summarized with the aim of providing a unifying perspective. At low supersonic Mach numbers, jets

will support only the Kelvin–Helmholtz and the subsonic instability waves. Within this Mach number range the Kelvin–Helmholtz instability waves have large growth rates and are the dominant instability of the jet flow. Supersonic instability waves exist only when the jet flow velocity exceeds the sum of the jet and ambient speed of sound, i.e. $u_j > a_j + a_0$ (equation (2.13)). Unlike Kelvin–Helmholtz instability which has a single wave mode for each azimuthal wave number, supersonic instability waves consist of a family of wave modes for the same azimuthal wavenumber. For clarity, therefore, each supersonic instability wave mode is designated by an azimuthal and a radial mode number. The relative dominancy of the Kelvin–Helmholtz instability and the supersonic instability is a function of the jet Mach number and the jet to ambient temperature ratio. Figure 9 shows the critical Mach number for a given temperature ratio below which the Kelvin–Helmholtz instability waves, having the largest growth rate, is the dominant instability. The critical Mach number arises because the spatial growth rates of the Kelvin–Helmholtz instability and the supersonic waves have exactly opposite jet Mach number dependence. It is well known that the Kelvin–Helmholtz instability becomes less and less unstable as the jet Mach number increases. On the other hand, numerical results obtained in the present investigation reveal that the maximum growth rate of the supersonic instability waves increases steadily with Mach number (at least up to $M_j = 5.0$). The same is true for jet temperature. The effect of increasing the mixing-layer thickness of the jet, in general, is to reduce the spatial growth rates of the instability waves. For jets with reasonably thick shear layer ($b/R_j = 0.1$ to 0.2) the growth rates of the higher-order supersonic instability waves are greatly reduced so that only the low-order wave modes are important. When restricted to cold jets with Mach number up to 5.0 the Strouhal number of the most unstable wave lies in the range 0.25–0.55. The maximum spatial growth rate per jet diameter is 0.2–0.4. On comparing with the spatial growth rate of instability waves of subsonic jets these are relatively weak instabilities. One of the most interesting findings of the present numerical study is that the phase or convection velocity of the most unstable supersonic instability wave non-dimensionalized by the jet velocity, as given by equation (5.1) (or equation (5.2) if the specific heat ratio of the gas of the jet is different from that of the ambient gas), is a function of the jet to ambient temperature ratio alone. That is to say, formula (5.1) is valid regardless of jet Mach number, mode number and mixing-layer thickness (say for b/R_j less than 0.3). According to the work of Papamoschou & Roshko (1986) there is also reason to believe that this formula is applicable even to moderately large-amplitude waves. The subsonic waves of supersonic jets are unstable only if the mixing layer has a finite (but small) thickness. The growth rates of these waves are very small. They are the least unstable waves. It is found, somewhat unexpectedly, that there is a branch of these waves which can propagate upstream following the jet even when the jet flow is supersonic. How important these waves are is not clear at this time. Further work is needed to clarify whether these waves play any role in the feedback cycle of a screeching imperfectly expanded jet or an impinging jet directed at a wall.

9. Discussion

In this paper three families of waves with distinct wave patterns and propagation characteristics have been identified in high-speed jets. They are the Kelvin–Helmholtz instability waves, the supersonic and the subsonic instability waves. At

subsonic speeds jets are subjected to only one type of instability, namely, the Kelvin–Helmholtz instability. For these jets it has been found that the Kelvin–Helmholtz instability waves are responsible for the formation of large turbulence structures in the jet flow. These large structures control the dynamics and mixing of the jet fluid. For supersonic jets at low to moderate supersonic Mach number experimental observations suggest that the flow is dominated by similar dynamical processes. Recently Lepicovsky, Ahuja & Brown (1987) provided photographic evidence of the existence of Kelvin–Helmholtz instabilty waves in these jets at Reynolds number of 10^6 and higher. In addition to being a key factor in the dynamics and mixing processes of moderately supersonic jets, Kelvin–Helmholtz instability waves have also been recognized to be the dominant source of jet mixing noise (see Troutt & McLaughlin 1982; Tam & Burton 1984). For imperfectly expanded jets the presence of a shock cell structure inside the jet flow leads to the radiation of additional noise. The additional noise consists of two components. One has discrete frequency and the other is broadband. They are generally referred to as screech tones and broadband shock associated noise (see Powell 1953; Davies & Oldfield 1962; Tam *et al.* 1986; Tam 1987). It has been shown that the additional noise components are generated by the interaction of the downstream propagating Kelvin–Helmholtz instability waves and the quasi-periodic shock cell structure (as the former pass through the latter). Thus the Kelvin–Helmholtz instability waves are important entities of a jet flow not only with respect to the dynamics and mixing processes but also in relation to the mechanisms of noise generation.

Now in this paper it has been found that at high supersonic Mach number a jet can support two other types of instability waves. What role then would these new instability waves play in the turbulence dynamics, mixing processes and noise generation of these jets? Furthermore, it was found in §2.4 that beyond the critical Mach number the Kelvin–Helmholtz instability waves would merge with the supersonic instability waves and that the supersonic instability waves were actually the dominant instabilities. What then would this imply concerning the spreading rate and the noise spectrum of a jet as the jet Mach number increases and passes the critical value? These are challenging questions which, however, are beyond the scope of the present investigation.

This paper was supported by NASA Grant NAG 1-421 and ONR Grant No 0014-07-J-1130 and the Florida State University through time granted on its Cyber 205 Supercomputer. The authors wish to thank Professor H. Oertel and the Directors of the Institute Franco-Allemand De Recherches De Saint-Louis for their generous cooperation and permission to reproduce figure 3 of ISL Report R 110/82.

Appendix. Flow over a wavy cylindrical wall

In this Appendix the flow over a cylindrical wavy wall as shown in figure 4 is considered. The flow inside is solved first. Then the flow outside with subsonic and supersonic velocity will be analysed.

A.1. *Supersonic flow inside a cylindrical wavy wall*

Let the jet Mach number be M_j and the radius of the cylindrical wall be R_j. Suppose the cylindrical surface is deformed radially into a wavy surface with radial displacement $r = \epsilon \sin \alpha x[\sin n\theta$ or $\cos n\theta]$ where (r, θ, x) are the cylindrical coordi-

nates with the x-axis coinciding with the axis of the cylinder. On starting from the linearized equations of motion the steady-state equation governing the perturbation pressure $p(r, \theta, x)$ is easily found to be,

$$M_j^2 \frac{\partial^2 p}{\partial x^2} - \nabla^2 p = 0. \tag{A 1}$$

The boundary condition on the wavy wall is

$$\frac{\partial p}{\partial r} = \epsilon \alpha^2 \rho_j u_j^2 \sin \alpha x \begin{Bmatrix} \sin n\theta \\ \cos n\theta \end{Bmatrix}. \tag{A 2}$$

The solution of (A 1) satisfying boundary condition (A 2) is

$$p_i(r, x, \theta) = \frac{\epsilon \alpha \rho_j u_j^2}{(M_j^2-1)^{\frac{1}{2}}} \frac{J_n((M_j^2-1)^{\frac{1}{2}} \alpha r)}{J_n'((M_j^2-1)^{\frac{1}{2}} \alpha R_j)} \sin \alpha x \begin{Bmatrix} \sin n\theta \\ \cos n\theta \end{Bmatrix}, \tag{A 3}$$

where $J_n(\ )$ is the Bessel function of order n.

A.2. Subsonic flow outside a cylindrical wavy wall

On proceeding as above it is easy to find that the pressure $p_o(r, \theta, x)$ outside a cylindrical wavy wall at subsonic flow Mach number, M_o is given by

$$p_o(r, \theta, x) = \frac{\epsilon \alpha \rho_o u_o^2}{(1-M_o^2)^{\frac{1}{2}}} \frac{K_n((1-M_o^2)^{\frac{1}{2}} \alpha r)}{K_n'((1-M_o^2)^{\frac{1}{2}} \alpha R_j)} \sin \alpha x \begin{Bmatrix} \sin n\theta \\ \cos n\theta \end{Bmatrix}, \tag{A 4}$$

where $K_n(\ )$ is the nth order modified Bessel function.

From (A 3) and (A 4) the pressure imbalance at the surface of a wavy cylindrical vortex-sheet jet is

$$\begin{aligned} \Delta p &= p_o(R_j, \theta, x) - p_i(R_j, \theta, x) \\ &= \epsilon \alpha \left[\frac{\rho_o u_o^2}{(1-M_o^2)^{\frac{1}{2}}} \frac{K_n((1-M_o^2)^{\frac{1}{2}} \alpha R_j)}{K_n'((1-M_o^2)^{\frac{1}{2}} \alpha R_j)} \right. \\ &\quad \left. - \frac{\rho_j u_j^2 J_n((M_j^2-1)^{\frac{1}{2}} \alpha R_j)}{(M_j^2-1)^{\frac{1}{2}} J_n'((M_j^2-1)^{\frac{1}{2}} \alpha R_j)} \right] \sin \alpha x \begin{Bmatrix} \sin n\theta \\ \cos n\theta \end{Bmatrix}. \end{aligned} \tag{A 5}$$

If α is chosen such that the terms inside the square brackets of (A 5) cancel each other then a wave with arbitrary amplitude ϵ becomes possible. For these α there are neutral wave modes. The existence of unstable modes is possible but not guaranteed since the unsteady effects of the flow have not been included in the model.

A.3. Supersonic flow outside a cylindrical wavy wall

For $M_o > 1$ similar consideration as above gives the following expression for the perturbation pressure

$$p_o(r, \theta, x) = \frac{\epsilon \alpha \rho_o u_o^2}{(M_o^2-1)^{\frac{1}{2}}} \operatorname{Im} \left\{ \frac{H_n^{(1)}((M_o^2-1)^{\frac{1}{2}} \alpha r)}{H_n^{(1)\prime}((M_o^2-1)^{\frac{1}{2}} \alpha R_j)} e^{i\alpha x} \right\} \begin{Bmatrix} \sin n\theta \\ \cos n\theta \end{Bmatrix}, \tag{A 6}$$

where $H_n^{(1)}(\ )$ is the nth order Hankel function of the first kind and $\operatorname{Im}\{\ \} =$ the imaginary part of. It is straightforward to show that at $r = R_j$ the pressure given by (A 6) cannot balance that of (A 3). Therefore, at supersonic convective Mach number no neutral waves are possible.

REFERENCES

BRIGGS, R. J. 1964 *Electron-Stream Interaction with Plasmas*. MIT Press.

CHAN, Y. Y. & WESTLEY, R. 1973 Directional acoustic radiation generated by spatial jet instability. *Can. Aero. & Space Inst. Trans.* **6**, 36–41.

COHN, H. 1983 The stability of a magnetically confined radio jet. *Astrophys. J.* **269**, 500–512.

DAVIES, M. G. & OLDFIELD, D. E. S. 1962 Tones from a choked axisymmetric jet. *Acoustica* **12**, 257–277.

FERRARI, A., TRUSSONI, E. & ZANINETTI, L. 1981 Magnetohydrodynamic Kelvin–Helmholtz instabilities Astrophysics – II. Cylindrical boundary layer in vortex sheet approximation. *Mon. Not. R. Astr. Soc.* **196**, 1051–1066.

GILL, A. E. 1965 Instabilities of Top-Hat jets and wakes in compressible fluids. *Phys. Fluids* **8**, 1428–1430.

LEPICOVSKY, J., AHUJA, K. K. & BROWN, W. H. 1987 Coherent large-scale structures in high Reynolds number supersonic jets. *AIAA J.* **25**, 1419–1425.

LIEPMANN, H. & PUCKETT, A. E. 1947 *Introduction to Aerodynamics of a Compressible Fluid*, pp. 239–241. John Wiley & Sons.

LIEPMANN, & ROSHKO, A. 1957 *Elements of Gas Dynamics*. John Wiley & Sons.

LOWSON, M. V. & OLLERHEAD, J. B. 1968 Visualization of noise from cold supersonic jets. *J. Acoust. Soc. Am.* **44**, 624–630.

MICHALKE, A. 1984 Survey on jet instability theory. *Prog. Aerospace Sci.* **21**, 159–199.

MILES, J. W. 1958 On the disturbed motion of a plane vortex sheet. *J. Fluid Mech.* **4**, 538–552.

MOORE, C. J. 1977 The role of shear layer instability waves in jet exhaust noise. *J. Fluid Mech.* **80**, 321–367.

OERTEL, H. 1979 Mach wave radiation of hot supersonic jets. In *Mechanics of Sound Generation in Flows* (ed. E. A. Muller), pp. 275–281. Springer.

OERTEL, H. 1980 Mach wave radiation of hot supersonic jets investigated by means of the shock tube and new optical techniques. *Proc. of the 12th Intl Symp. on Shock Tubes and Waves, Jerusalem* (ed. A. Lifshitz & J. Rom), pp. 266–275.

OERTEL, H. 1982 Coherent structures producing Mach waves inside and outside of the supersonic jet. Structure of complex Turbulent Shear Flow. *IUTAM Symp. Marseille.*

PAPAMOSCHOU, D. & ROSHKO, A. 1986 Observations of supersonic free shear layers. *AIAA paper* 86-0162.

PAYNE, D. G. & COHN, H. 1985 The stability of confined radio jets: the role of reflection modes. *Astrophys. J.* **291**, 655–667.

POWELL, A. 1953 On the mechanism of choked jet noise. *Proc. Phys. Soc. Lond.* B**66**, 1039–1056.

ROSALES, A. A. 1970 Shadowgraphic observation of the acoustic field and structure of cold axisymmetric supersonic jets. MS thesis, Dept of Aero. & Astro. MIT.

TAM, C. K. W. 1971 Directional acoustic radiation generated by shear layer instability. *J. Fluid Mech.* **46**, 757–768.

TAM, C. K. W. 1987 Stochastic model theory of broadband shock associated noise from supersonic jets. *J. Sound Vib.* **116**, 265–302.

TAM, C. K. W. & BURTON, D. E. 1984 Sound generated by instability waves of supersonic flows. Part 2. Axisymmetric jets. *J. Fluid Mech.* **138**, 273–295.

TAM, C. K. W. & HU, F. Q. 1988 The instability and acoustic wave modes of supersonic mixing layers inside a rectangular channel. Submitted to *J. Fluid Mech.*

TAM, C. K. W., SEINER, J. M. & YU, J. C. 1986 Proposed relationship between broadband shock associated noise and screech tones. *J. Sound Vib.* **110**, 309–321.

TROUTT, T. R. & MCLAUGHLIN, D. K. 1982 Experiments on the flow and acoustic properties of a moderate Reynolds number supersonic jet. *J. Fluid Mech.* **116**, 123–156.

ZANINETTI, L. 1986 Numerical results on instabilities of top hat jets. *Phys. Fluids* **29**, 332–333.

ZANINETTI, L. 1987 Maximum instabilities of compressible jets. *Phys. Fluids* **30**, 612–614.